Semi-annual Progress Report for NASA grant NAG-1-1057

In situ detection of tropospheric OH, HO_2, NO_2, and NO by laser-induced fluorescence in detection chambers at reduced pressures

For the period: 1 April, 1993 to 30 September, 1993

Principal Investigator: William H. Brune

Department of Meteorology
Pennsylvania State University
University Park, PA 16802

26 December, 1993

This report is a brief summary of the status of work on the grant entitled "In situ detection of tropospheric OH, HO_2, NO_2, and NO by laser induced fluorescence in detection chambers at low pressures." The basic instrument characteristics have been established, and have been reported in a manuscript, included as an appendix to this report, that has been accepted by the *Journal of Geophysical Research.* Currently, two efforts are under way. First, instrument tests and calibrations are continuing. These efforts include field measurements and an informal intercomparison in Colorado last August and September. Second, new technologies in lasers and detectors are being implemented to make the instrument smaller, lighter, and more energy efficient. Such instrument modifications are essential for measurements from aircraft, high scaffolding in forests, and ships.

Activities of the last six months

Much of our effort for the last six months was the preparation and participation in an informal intercomparison at Idaho Hill, near Caribou, Colorado. We were informally intercomparing with two other instruments: the chemical ionization/mass spectrometer instrument of Eisele and coworkers and the long-path absorption instrument of Mount and coworkers. Measurements were made of other variables, including NO_x, O_3, RO_2, CO, water vapor, hydrocarbons, sulfur compounds, particles, j-values for NO_2 and $O(^1D)$, and meteorological parameters.

For this experiment, we decided to house the laser system in a trailer that became available to us at the Department of Meteorology. This configuration was different from either the one we had used on the roof of the Walker Building in 1991 for the initial tests or the one we used in rural Alabama in June, 1992 for the ROSE II experiment. This trailer housed the laser and electronics. The detection cell was placed on top of a tower, which was attached to the end of the trailer and rose 1 meter above the roof of the trailer. The ultraviolet light from the laser was sent to the detection cell through a quartz window in the roof of the trailer.

We chose to use a new dye laser, copying the successful design that is being used by Harvard University for their OH/HO_2 instrument on the NASA ER-2. However, as discussed in the proposal, we decided to excite this dye laser with the copper laser from Oxford Lasers for this informal intercomparison. This combination of lasers has been used successfully at Harvard University for a number of years in the kinetics laboratories.

This dye laser has several advantages over the Lambda Physik dye laser. First, it is much smaller and lighter, and is part of our plan the reduce the size, weight, and power requirements of our system to increase its usefulness. Second, it is more efficient. Third, it is capable of producing a narrower laser spectral line width, thus giving more sensitivity, while maintaining the necessary laser power.

We received the dye laser in late April from Harvard. Unfortunately, the combination of the Oxford Lasers copper laser and the Harvard dye laser produced less that 0.5 mW of UV power, and during the Colorado experiment, often produced less than 0.2 mW. This laser power was about a factor of 50 to 100 less than we or the scientists at Harvard had anticipated. Despite significant efforts, we were unable to increase the power for the Colorado experiment, although we are confident that more experimentation with the optics

and dye solutions will eventually lead to the expected laser power.

Despite these problems with the dye laser, we were able to make some major improvements to our detection system for this informal intercomparison. First, the White cell was made much more stable, so that after the initial alignment no further adjustments were required. Second, the thermal control and weather resistance of the instrument was improved. Third, a new calibration monitor, Raman scattering from the nitrogen inside the detection cell, was implemented. When this monitor is fully operational, we will be able to track the instrument calibration on a second-by-second basis. Finally, a new, highly reliable pumping system consisting of four small pumps was used, resulting in reduced weight, starting power, and operating power and greater versatility.

We were at the site in Colorado from 11 August to 23 September, and made measurements for all or part of 25 days. HO_2 was measured for 25 days, and OH for 9 days. Because of the low laser power, typical values for minimum detectable OH (S/N = 2) were 5×10^6 OH molecules cm^{-3} for 1 minute and 7×10^5 cm^{-3} for 1 hour. Thus, HO_2 detection was possible in a few seconds, while OH detection required about an hour. Since our return from Colorado, we have concentrated on the instrument calibration, the conversion of HO_2 to OH, and the development of data analysis routines. As a result, not all the data are analyzed.

We have some preliminary numbers for two days, 12 and 20 September (Figures 1 and 2). The top section is the HO_2 measurements, which have been averaged into roughly 5 minute intervals. Peak values of 0.5 to 1.5 $\times 10^8$ HO_2 molecules cm^{-3} are fairly typical for our measurements in Colorado. Because the air pressure at Caribou was $\sim 1.7 \times 10^{19}$ molecules cm^{-3}, typical peak values of the HO_2 mixing ratio were 3 to 10 pptv. These levels are lower than expected by as much as a factor of 2 to 5.

The preliminary OH measurements in the second panel of each figure are shown with the 2σ statistical error bars (vertical) and the time of integration (horizontal error bars). The data are noisy because of the low detection sensitivity, but the values are generally a few times 10^6 cm^{-3}. It is anticipated that we will have about 20 to 30 OH data points that we can compare with Eisele and Mount.

We have spent the last two months since the end of the informal intercomparison calibrating and testing the instrument. The laser system and detection cell were removed from the trailer and set-up in the same configuration in the laboratory. These laboratory calibrations and tests are in excellent agreement with those made in the field.

First, the calibrated detection sensitivity, per milliwatt of laser power, was found to be 3×10^{-6} (cts s)/(cm^{-3} mw), using the known photolysis of water vapor as the calibration procedure. The uncertainty in this calibration method has been reduced from a factor of 1.5 to a factor of 1.35 by the improvement in the velocity profile of the flow of nitrogen in the calibration system.

Second, the OH and HO_2 signals were equal to within 10% when equal amounts of OH and HO_2 were created by the photolysis of water vapor. This equality suggests that the conversion of HO_2 to OH is close to 100%. This result is confirmed by a test in which OH is converted into HO_2 by reaction with reagent CO, and is then converted back to OH

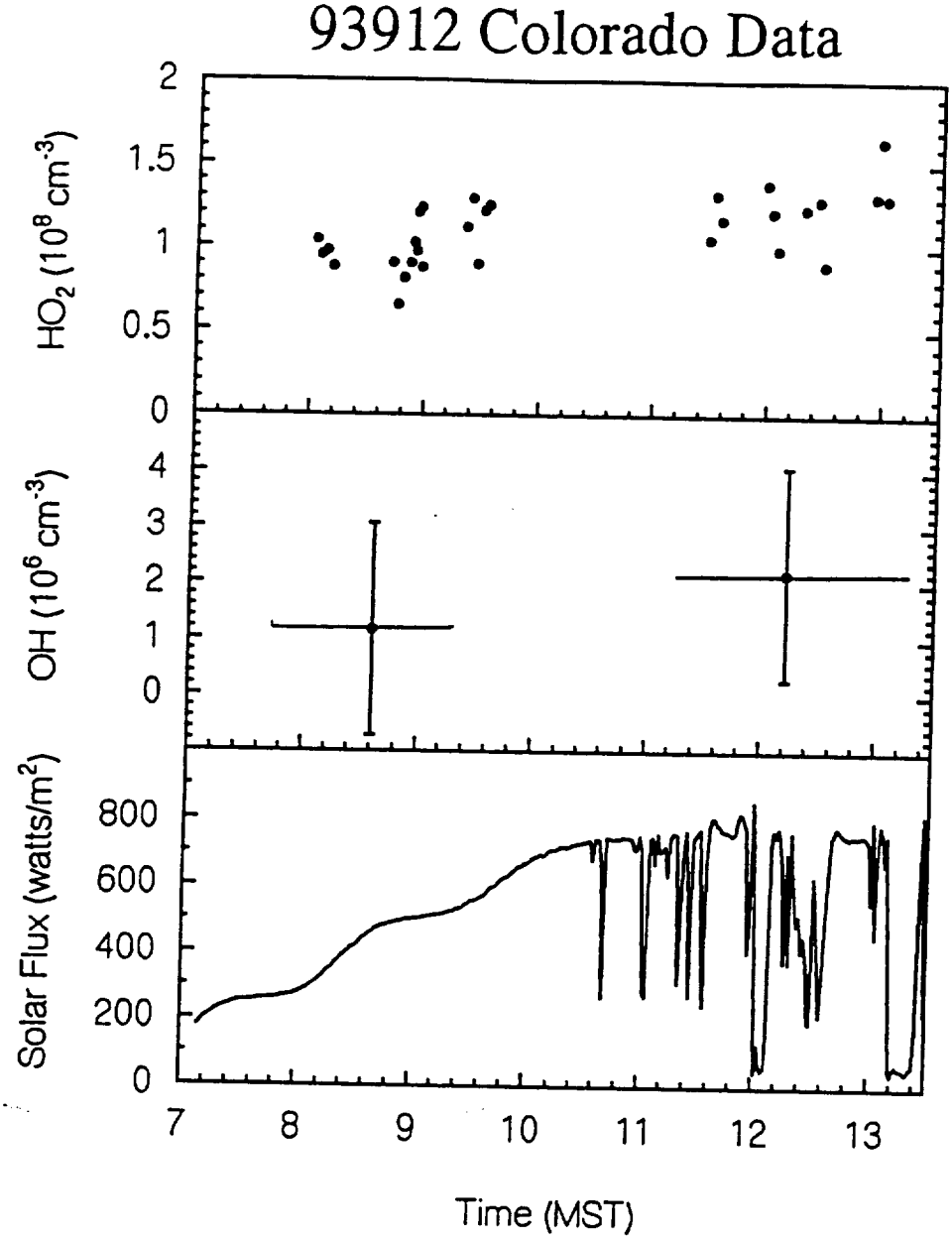

Figure 1. Measurements of OH, HO_2, and sunlight for 12 September, 1993, during the Colorado informal intercomparison. The horizontal bars on the OH values indicate the span over which the measurements were averaged. The vertical bars indicate the 2σ uncertainty. The oscillations in the solar flux are due to instrument artifacts.

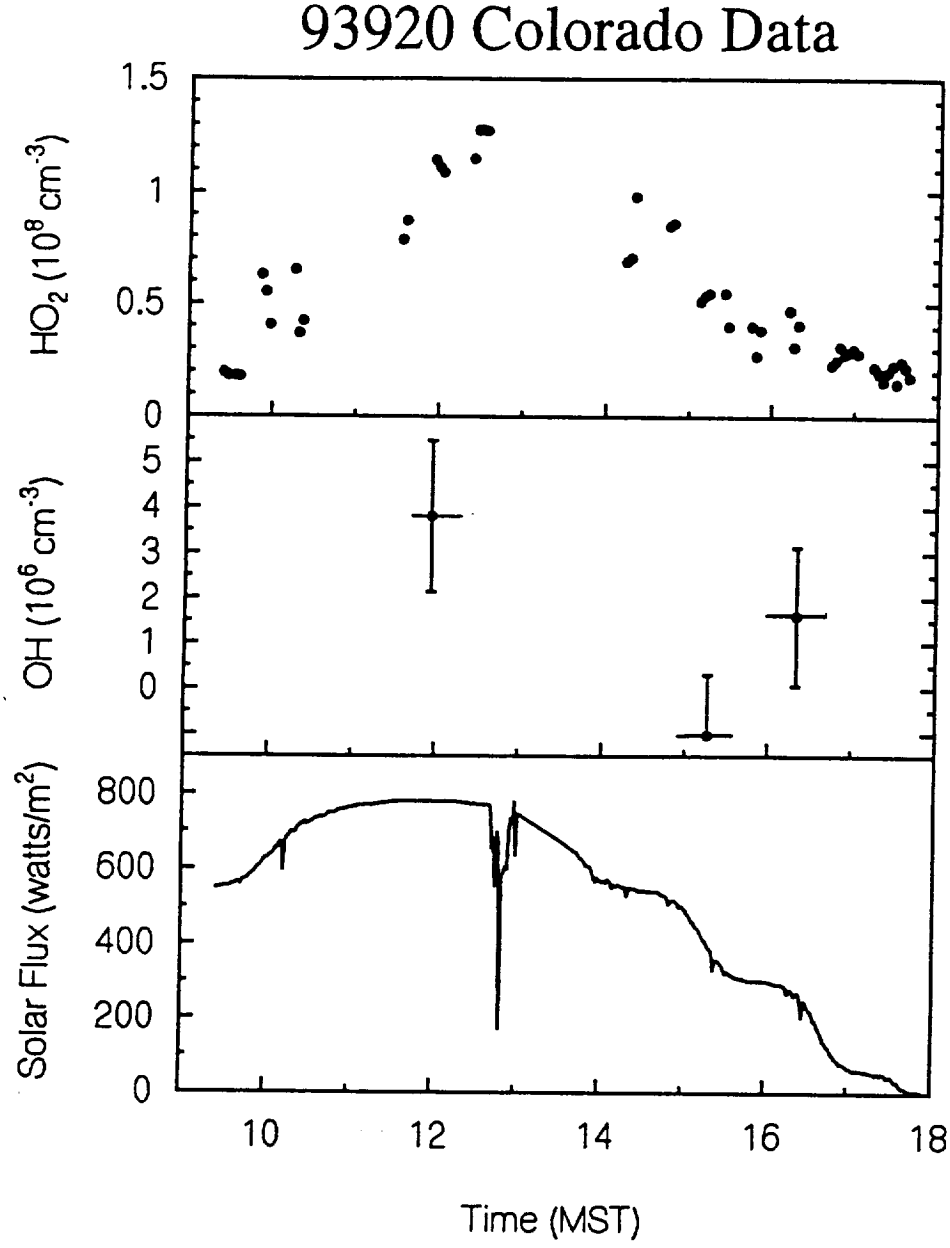

Figure 2. Measurements of OH, HO_2, and sunlight for 20 September, 1993, during the Colorado informal intercomparison. Error bars on OH are the same as for Figure 1. The reason for the near-zero value of OH has not been explained.

inside the detection system by reaction with reagent NO.

The confirmation in the laboratory of the tests performed during the Colorado informal intercomparison suggest that our observed low values for HO_2 are correct. These low values seem inconsistent with theoretical expectations and the results of other measurements, and we continue to search for potential problems in our approach.

A postdoctoral fellow and a graduate assistant have been working on these OH and HO_2 measurements. The graduate assistant, James H. Mather, defended his Ph. D. dissertation on 16 December, 1993, and is now leaving to take a post doctoral position. A new graduate assistant will be recruited to continue his efforts.

A second graduate assistant, Ching Fong, continues to develop a prototype instrument for the detection of NO_2 by laser induced fluorescence. Once small, room-temperature diode lasers are available at wavelengths near 585 nm, this LIF detection technique could become a cost-effective and reliable method for measuring NO_2 and NO. Therefore, it is worthwhile to do the groundwork for this development now with a dye laser system. All the major components of the system, with the exception of the computer control, have been purchased and assembled. Much of the effort in the last six months has been to get the copper laser and dye laser working properly in the wavelength regions of interest. This effort is continuing.

Planned activities for the next six months

In the next two months, we continue to work on the instrument calibration and the conversion efficiency for HO_2 to OH. A system will be built to add a known amount of OH in a horizontal flow, perpendicular to the instrument inlet. In this way, we will test for possible losses of OH and HO_2 for the conditions of the measurements. In this prototype system, we will be limited to a flow of less than 1 m s^{-1}. Later versions will have higher flow rates. We will also use the absorption calibration method as another test.

We will also begin a more thorough analysis of the observations from the Colorado informal intercomparison and from ROSE II. The goal is to retrieve OH and HO_2 values from both data sets before the meeting for the Colorado informal intercomparison in Boulder at the end of February. The second goal of this effort is to analyze instrument performance during the intercomparison. We are particularly interested in the dependence of the HO_2 signal on wind speed and direction, laser power, and amount of NO reagent. Other studies will focus on the consistency among the various laser power monitors, Rayleigh and Raman scattering, and on operational characteristics.

The third effort of the next six months is to identify the problem with the Oxford Lasers copper laser and Harvard dye laser combination. We will examine the effects of focusing of the copper laser beam into the dye laser, the effects of different dye combinations and solvents, and the effects of the position and material of the tuning prisms inside the dye laser. Our goal is to get the dye laser to work with the green line (510 nm) from the copper laser and not the yellow line (578 nm), which we used in Colorado. Successful completion of this work is necessary before we can make more field measurements or change the

excitation laser from the copper laser to an all solid state laser.

Once we get the laser to produce a stable 10 to 20 mW of ultraviolet light, then we will put the system back in the trailer and take it out to Rock Springs, a meteorological field station in the middle of Penn State agricultural lands, a few miles from the campus. This effort may not occur until the middle to end of the summer, depending on the time it takes to improve the laser performance. At Rock Springs, we will study in greater detail the effects of the environment on the measurement of OH and HO_2. We expect to obtain signals for OH and HO_2 similar to those obtained in March, 1992. We will do the initial test of measuring the flux of HO_2 using the eddy correlation technique.

For the NO_2 detection system, efforts will be concentrated in two areas. First will be work on the laser output. Approximately one watt of laser power must be produced with a narrow line width (0.04 cm^{-1}) in a wavelength region were NO_2 has strong, discrete absorption features. Second will be work on developing filters to isolate the laser excitation light from the NO_2 fluorescence that extends to the red of the excitation. When these two goals are reached, then the system will be ready for testing, either on the roof of the Walker Building or at Rock Springs. We anticipate that this instrument will be making atmospheric measurements by the end of the year.

Finally, we have proposed to both the NOAA Climate and Global Change Program and the NASA Subsonic Assessment (SASS) program for funds to adapt our instrument to aircraft use. This effort would occur in addition to the measurements and studies that I have already described. To make this adaption, we will need to acquire a new solid state laser to excite the dye laser within the next six months to a year. We envision developing an instrument, based on this smaller laser system, that can be used on a variety of platforms with changes only to the housing and the orientation of the inlet. All of the components would be used in these different configurations. We would create this new instrument during the next year and a half, so that it would be available for atmospheric measurements by the end of 1995.

Appendix A. A manuscript accepted for publication by the *Journal of Geophysical Research.*

Measurement of Tropospheric OH and HO_2 by Laser-Induced Fluorescence at Low Pressure

P.S. Stevens, J.H. Mather and W.H. Brune
Department of Meteorology, The Pennsylvania State University, University Park, Pennsylvania

Abstract

The hydroxyl radical (OH) is the primary oxidant in the atmosphere, responsible for many photochemical reactions that affect both regional air quality and global climate change. Because of its high reactivity, abundances of OH in the troposphere are less than 1 pptv, and thus difficult to measure accurately. This paper describes an instrument for the sensitive detection of OH in the troposphere using low-pressure laser-induced fluorescence. Ambient air is expanded into a low-pressure detection chamber, and OH is both excited and detected using the $A^2\Sigma^+(v' = 0) \rightarrow X^2\Pi(v'' = 0)$ transition near 308 nm. An injector upstream of the detection axis allows for the addition of reagent NO to convert ambient HO_2 to OH using the fast reaction $HO_2 + NO \rightarrow OH + NO_2$. Using recent advances in laser and detector technologies, this prototype instrument is able to detect less than 1×10^5 molecules cm^{-3} (0.004 pptv) of OH with an integration time of 30 seconds with negligible interferences.

Introduction

One of the most important species in tropospheric photochemistry and global climate change is the hydroxyl radical (OH). Reactions with OH are the primary loss mechanisms for a number of important species, such as methane and the alternative chlorofluorocarbons (HCFC's), which contribute to global warming and stratospheric ozone depletion. As a result, the lifetimes for these species are dependent on the OH concentration. In addition, OH initiates the oxidation of carbon monoxide and hydrocarbons, which in the presence of nitrogen oxides, produce ozone, peroxyacetylnitrate (PAN) and other pollutants. Because of this central role in atmospheric photochemistry, the hydroxyl radical is responsible for processes which occur on local, regional and global scales.

Despite the importance of OH in tropospheric photochemistry, very little is known about its abundance, and if it is changing over time. OH is formed in the troposphere from the photolysis of ozone and subsequent reaction of $O(^1D)$ with water vapor [*Logan et al.*, 1981; *Trainer et al.*, 1987]:

$$O_3 + h\nu\ (< 310nm) \rightarrow O(^1D) + O_2(^1\Delta_g) \quad (1)$$

$$O(^1D) + H_2O \rightarrow OH + OH \quad (2)$$

OH in the troposphere is primarily removed by reactions with carbon monoxide and methane,

$$OH + CO \rightarrow CO_2 + H \quad (3a)$$

$$H + O_2 + M \rightarrow HO_2 + M \quad (3b)$$

$$OH + CH_4 \rightarrow H_2O + CH_3 \quad (4a)$$

$$CH_3 + O_2 + M \rightarrow CH_3O_2 + M \quad (4b)$$

converting OH to the hydroperoxy radical (HO_2) and the methoxy radical (CH_3O_2). Similar to the reaction with methane, OH oxidizes many hydrocabons, forming other peroxy radicals (RO_2). HO_2 and RO_2 are rapidly cycled back into OH through reactions with nitric oxide, ozone, and O_2, resulting in a photochemical equilibrium between OH and HO_2/RO_2:

$$HO_2 + NO \rightarrow OH + NO_2 \quad (5)$$

$$HO_2 + O_3 \rightarrow OH + 2O_2 \quad (6)$$

$$RO_2 + NO \rightarrow RO + NO_2 \quad (7)$$

$$RO + O_2 \rightarrow R'HO + HO_2 \quad (8)$$

Since the recognition of the important role the OH radical plays in tropospheric chemistry [*Weinstock et al.*, 1969; *Levy*, 1971; *Crutzen*, 1974], many attempts have been made to measure its abundance over the past 20 years. Because of the high reactivity of OH, predicted mixing ratios in the troposphere are extremely small (less than 0.5 pptv, $\sim 1 \times 10^7$ molecules cm^{-3}) [*Logan et al.*, 1981; *Perner et al.*, 1987]. These predictions are in reasonable agreement with empirically derived OH abundances determined from chemical lifetime measurements of methyl chloroform, a compound with well known anthropogenic sources [*Prinn et al.*, 1987]. Methyl chloroform is removed from the atmosphere by reaction with OH, and thus its lifetime is directly related to the OH abundance. However, because the lifetime of methyl chloroform in the atmosphere is long (6 years), OH concentrations derived in this manner reflect global average abundances. Although OH concentrations derived from this empirical method are extremely valuable, they have yet to be verified by direct measurements. In addition, uncertainties in source strengths and oceanic losses for methyl chloroform prevent a rigorous test of photochemical models.

The small mixing ratios of OH in the troposphere are extremely difficult to measure accurately, especially on the short time scale required as a test of the rapid photochemistry of OH. Early local measurement attempts were plagued by interferences and uncertainties [*Ortgies et al.*, 1980; *Davis et al.*, 1981 a,b], and as a result, theoretical models of tropospheric OH have advanced far beyond the experimental measurements. However, a number of local measurement techniques have advanced to the point where reliable OH measurements are now being made, and are ready to provide a true test of photochemical theories. A recent intercomparison between two different OH measurement techniques resulted in measured OH concentrations substantially below model predictions [*Mount and Eisele*, 1992]. This discrepancy suggests that our knowledge of tropospheric photochemistry may be incomplete, thus limiting our ability to predict with confidence how changes in the composition of the atmosphere may affect global climate change in the future [*Thompson*, 1992].

Methods for detecting OH locally in the troposphere include spectroscopic and non-spectroscopic approaches (for a review, see *O'Brien and Hard*, 1993). Spectroscopic techniques include laser-induced fluorescence [*Bradshaw et al.*, 1984; *Hard et al.*, 1984, 1986; *Shirinzadeh et al.*, 1987; *Chan et al.*, 1990;

Hofzumahaus et al., 1990] and long-path absorption [*Dorn et al.*, 1988; *Armerding et al.*, 1990; *Hofzumahaus et al.*, 1991; *Mount*, 1992]. These techniques have the advantage of specificity, however in the past they have suffered from background interferences which limited the overall sensitivity of the instruments. Non-spectroscopic techniques rely on chemical conversion of OH to a species which is more easily detected, such as the ion-assisted method [*Eisele and Tanner*, 1991], and the radiocarbon CO method [*Felton et al.*, 1990]. Although highly sensitive, these techniques require careful analysis to prevent spurious OH production in the titration scheme. With the exception of long-path absorption, all OH measurement techniques require careful calibrations to account for interactions of the sampling process with ambient air.

Methods for detecting HO_2 in the troposphere also include both spectroscopic and non-spectroscopic approaches. Non-spectroscopic techniques include chemical conversion to OH [*Hard et al.*, 1992a], and chemical amplification of both HO_2 and RO_2 through a series of chain reactions followed by detection of NO_2 [*Cantrell et al.*, 1984; *Hastie et al.*, 1991]. Spectroscopic techniques include matrix isolation/ESR detection of HO_2 [*Mihelcic et al.*, 1990], as well as infrared absorption [*Nelson and Zahniser*, 1991].

Laser-induced fluorescence (LIF) remains a promising technique for the detection of OH, offering both high sensitivity and selectivity. Although OH has been measured successfully in the stratosphere and lower mesosphere using fluorescence techniques [*Anderson*, 1976; *Stimpfle and Anderson*, 1988; *Stimpfle et al.*, 1989], applications of these techniques to tropospheric OH measurements has been difficult. Initial attempts utilized the $A^2\Sigma\ v' = 1 \leftarrow X^2\Pi\ v'' = 0$ electronic transition of OH at 282 nm, and observed the red-shifted fluorescence from the $A^2\Sigma\ v' = 0 \rightarrow X^2\Pi\ v'' = 0$ band near 308 nm [*Wang et al.*, 1976; *Davis et al.*, 1976]. The advantage of using this transition is that it easily allows the spectral isolation of the fluorescence from scattering of the laser pulse. Although this approach works well in the stratosphere, the high concentration of both water vapor and ozone in the troposphere results in the generation of OH by the laser itself through reactions (1) and (2), and broad-band fluorescence of other species excited by the 282 nm radiation added to the background signals [*Ortgies et al.*, 1980; *Davis et al.*, 1981 a, b]. These interferences proved to be quite severe, producing background OH signals which were often higher than ambient, reducing the overall sensitivity of these instruments.

A number of techniques have been introduced to reduce these interferences. One of the most notable of these is the sampling of ambient air at low pressure through an inlet. This technique was first developed by Hard *et al.* [1984] and called FAGE (Fluorescent Assay by Gas Expansion). Sampling ambient air at a low pressure reduces the concentration of interferring species, such as O_3 and H_2O, thus reducing the chemical reaction rates that produce OH from the laser pulse. The total signal resulting from OH fluorescence does not change appreciably because the reduction in OH concentration upon expansion is offset by the decreased collisional quenching rate at the lower pressure, which results in an increased quantum yield for fluorescence. The decreased collisional quenching rate at the low pressure also results in an increased lifetime of the OH excited state, which extends the fluorescence beyond the length of the laser pulse. Thus OH fluorescence, which lasts a few hundred nanoseconds, can be discriminated by electronic gating from Rayleigh and Mie scattering, chamber scatter, and fluorescence from species such as SO_2 and CH_2O, which have shorter radiative lifetimes.

Although low-pressure sampling greatly reduced much of the interference previously encountered, early versions of the FAGE technique still suffered from high background signals due to laser-generated OH [*Hard et al.*, 1984, 1986; *Chan et al.*, 1990]. Performing the excitation at 282 nm with a low repetition-rate laser system, with high energy per pulse, resulted in interference signals which were higher than ambient levels by a factor of 23 [*Smith and Crosley*, 1990]. Although the contribution of this interference to the total signal was determined through chemical removal of ambient OH in the flow system, the presence of these high backgrounds presented a significant limitation to the sensitivity of the instrument.

By using a high repetition-rate laser, with low energy per pulse, the internally generated OH can be reduced without sacrificing overall sensitivity. With a high average power, a higher repetition-rate laser system maintains a high OH fluorescence signal. The disadvantage of using a high repetition-rate laser is that it requires a high flow velocity in the detection region to prevent exposure of the same air mass to multiple pulses of the laser beam, which could lead to OH generation.

The laser-generated OH interference can be further reduced, but not eliminated, by both exciting and detecting in the $A^2\Sigma\ v' = 0 \rightarrow X^2\Pi\ v'' = 0$ band near

308 nm. The photodissociation of O_3 at 308 nm is reduced a factor of 25 when compared to excitiation at 282 nm [*DeMore et al.*, 1992]. In addition, the quantum yield of $O(^1D)$ may be lower at 308 nm Hard et al., 1992b, although there is still uncertainty associated with the production of $O(^1D)$ in this region DeMore et al., 1992. The disadvantage of this approach, as mentioned above, is the difficulty in isolating the OH fluorescence signal from scattered radiation.

Despite the difficulties mentioned above, the use of high repetition-rate laser systems, and excitation of OH at 309 nm and at low pressure has become a promising LIF technique for the fast and specific detection of OH in the troposphere. The present version of FAGE [*Chan et al*, 1990], as well as a similar instrument under development by Hofzumahaus *et al.* [1990] are incorporating these approaches. This paper describes a LIF instrument, based on the FAGE technique, which is capable of measuring OH and HO_2 in the troposphere with insignificant interferences. Using recent advances in laser and detection technologies, this instrument is capable of detecting less than 1×10^5 OH molecules cm^{-3} (0.004 pptv) with a S/N = 2 in 30 seconds.

Instrument Description

The instrument consists of (1) a laser system to generate the excitation radiation, (2) the OH sampling chamber, (3) a fast, gated detector and collection optics. The prototype instrument, used to make ambient measurements on the roof of the Walker Building at the University Park campus of the Pennsylvania State University, is shown in Figure 1.

Laser System

A 15-W, air cooled copper-vapor laser (Oxford Lasers), operating at 10 kHz and equipped with an unstable resonator, pumps a grating-tuned dye laser (Lambda Physik FL-3001). The output of the dye laser is frequency doubled from the red at 616 nm into the UV using a KDP crystal. The dye solution consists of a mixture of Rhodamine 640 (0.15 gm/L, Exciton), and Kiton Red (0.4 gm/L, Exciton) in ethanol. This dye mixture maximizes production of 616.5 nm (red) radiation from both the 510 nm (green) and 578 nm (yellow) output of the copper-vapor laser. At peak operating conditions, approximately 50-mW of doubled UV (20-nsec pulse length, 0.15-cm^{-1} line width) is produced from approximately 1 W of 616 nm output from the dye laser and 12-15 W from the copper-vapor laser. Typical operating conditions were at lower UV power to prevent saturation of the OH transition. A glan-laser prism separates the vertically polarized undoubled red fundamental beam from the horizontally polarized UV beam.

Before exiting the dye laser, the UV beam passes through an evacuated cell where OH is generated through thermal dissociation of ambient H_2O. This cell provides a resonance fluorescence OH signal as a reference to indicate when the dye laser is tuned into resonance with the OH transition. A 25-W alumel filament produces the reference OH, and the fluorescence is detected at approximately 1 torr using a Hamamatsu 760 photomultiplier tube located directly opposite of the filament. The detector is equipped with an interference filter and a UG-11 color-glass filter which isolates the fluorescence from the glowing filament.

Sampling Chamber

After exiting the dye laser, the UV beam is focussed into a White cell inside the sampling chamber. The optical layout is shown schematically in Figure 2. The beam crosses the air stream in 24 non-overlapping 2-mm by 5-mm beams at the center of the cell, separated along the direction of the flow by less than 10 mm. The UV laser power is monitored at the exit of the White cell.

Ambient air is introduced into the sampling chamber through a 0.93-mm diameter inlet centered on a flat plate. Pressure inside the chamber is maintained at 3.5 torr, with 0.5 torr from the addition of dry nitrogen or argon gas at the White cell mirrors. The volumetric flow rate inside the chamber is 35 liters sec^{-1}. The additional flow perpendicular to the flow, and along the axis of the White cell, serves to keep the White cell mirrors clean and to fill the detection volume, confining the ambient air stream to the center of the chamber. An injector, located directly below the inlet and 9-20 cm upstream of the detection axis is used for chemical addition. The inside of the chamber is coated with Teflon to reduce radical loss; however air that passes through the detection region does not contact these walls. A schematic of the internal flow is shown in Figure 3. The initial configuration of the instrument placed the inlet 11 cm above the detection axis (Figure 3a). The jet passed through a 5-cm diameter, 7.6-cm length flow tube before entering the nominally 7.6-cm diameter detection region, 3.8 cm above the laser beam path. Based on Schlieren studies the jet undergoes a shock 1-2 cm below the inlet.

Laboratory pitot tube studies of the jet in this configuration suggest that the flow is still supersonic at the detection axis (314 m sec^{-1}). Based on this velocity, the jet temperature, calculated from isentropic ideal gas equations is 245 K [*Shapiro*, 1958], approximately 50 K below ambient. This cooling of the jet will have a small (5%) effect on the density and the population of the absorbing level for the $Q_1(3)$ transition.

Subsequently, the inlet and injector were raised an additional 10 cm with a 5-cm diameter flow tube insert to increase the reaction time for chemical conversion (Figure 3b). The velocity of the jet at the detection axis was reduced to 70 m sec^{-1}. Fast themistor measurments of the temperature in this configuration, as well as the OH excitation spectra, suggest that the jet temperature has warmed to ambient. The velocity in this configuration is still greater than the 50 m sec^{-1} minimum velocity required to prevent exposure of the same air mass to multiple pulses of the 10 kHz laser beam. A 124 cfm mechanical pump (Leybold #S160) provides the flow velocity.

HO_2 is detected by the addition of NO to the air stream to convert ambient HO_2 to OH using reaction (5) ($k_{298} = 8.6\times10^{-12}$ cm^3 $molecule^{-1}$ sec^{-1} [*DeMore et al.*, 1992]). NO (Matheson, CP grade) is added through the injector located directly below the inlet (Figure 3). The NO passes through an Ascarite trap before injection into the system. Typical flow rates of NO are 0.04 to 1 sccs.

Detector and Collection Optics

The OH fluorescence is collected at right angles to both the air flow and the laser beams through an f#1 optical train, and focussed onto a Hamamatsu microchannel plate (MCP) detector (R2024U-06) (Figure 2). This detector has a 18-mm photocathode, recessed in the surrounding housing by 17 mm. To prevent vignetting, a 150-mm focal length diverging lens in front of the detector collimates the fluorescence onto the photocathode. The collimated fluorescence passes through a 25-mm UG-11 filter, which is 65% transmitting at 308 nm, and a 25-mm interference filter which is described in detail below.

The gain of the detector is normally reduced a factor of 9000 by a potential grid between the photocathode and the microchannel plate. The detector is turned on (rise time = .23 nsec) by applying a 12 V bias to the control grid approximately 30 nsec after each laser pulse has exited the White cell, and remains on for 300 nsec to collect the OH fluorescence. Thus, the OH fluorescence is isolated from Rayleigh and chamber scatter.

Although the current gain and quantum efficiency of the micro-channel plate (MCP) detector (5×10^5 and 5-6%) are both less than that for a photomultiplier tube (typically 2×10^6 and 20%), the loss of photon sensitivity is offset by the low background signals associated with the gating system of the MCP. A memory of the high Rayleigh scatter associated with the laser in a photomultiplier tube results in a high background signal long after the pulse [*Chan et al.*, 1990; *Crosley*, 1992]. The ability to quickly turn on the MCP after the laser pulse without any associated memory or ringing increases the ultimate OH detection sensitivity of this system.

The output signal of the MCP is amplified by a 280 MHz preamplifier (Stanford Research Systems SR440) with an overall gain of 91. The amplified signal is then counted by a 200 MHz gated photon counter with a built-in discriminator (Stanford Research Systems SR400). The counter gate is opened 40-50 nsec after the laser pulse, 10-20 nsec after the detector gate.

Instrument Performance

Several concerns must be addressed in order to assess the performance of a LIF instrument based on the FAGE technique: sensitivity, selectivity, minimum detectable OH, calibration, including HO_2 conversion efficiency, and interferences, including laser generated OH and detection of other species.

Sensitivity and Selectivity

The detection sensitivity, C, is given as the signal due to OH fluorescence divided by the OH concentration:

$$C = S_{OH}/[OH] \tag{9}$$

The detection sensitivity is dependent on the excitation rate, the collection efficiency of the optics and detector, the fraction of molecules in the excited state which radiate, and the density change upon expansion of air into the sampling chamber. The overall sensitivity of the instrument is also dependent on the transmission OH and HO_2 through the inlet. This issue will be treated separately below. The governing equation for the sensitivity is given by:

$$C = \left[\frac{B'_{j2}}{c^3}\left(\frac{4\ln 2}{\Pi}\right)^{1/2}\left(\Delta\nu_D^2 + \Delta\nu_l^2\right)^{-1/2}\frac{\Delta N}{N}\cdot P\cdot l\right] [\epsilon\cdot\eta\cdot T\cdot f_{gate}]\, Q\cdot\frac{\rho_{in}}{\rho_{amb}} \tag{10}$$

S_{OH}	detector signal in counts sec^{-1}.
B_{12}	Einstein B-coefficients for absorption [*Dimpfle and Kinsey*, 1979].
$\Delta\nu_D$ and $\Delta\nu_l$	OH Doppler and the laser line widths, respectively.
P	laser power in watts.
$\Delta N/N$	fraction of OH molecules in the rotational level being excited (calculated).
ϵ	collection efficiency of the optical train (calculated).
T	transmission of the optics (measured and estimated).
η	quantum yield of the detector (measured).
l	length of the laser beam overlapping the ambient air stream (calculated).
Q	quenching of the OH excited state [*German*, 1975; 1976; *Copeland and Crosley*, 1986; *Cleveland and Wiesenfeld*, 1988; *Wysong et al.*, 1990].
f_{gate}	fraction of the OH fluorescence collected (measured).
ρ_{in}/ρ_{amb}	ratio of air densities inside and outside the sampling chamber (measured).

A number of uncertainties are associated with the calculated sensitivity of the instrument, most notably the actual overlap of the laser beam with the ambient airstream, and the actual field of view of the detector. The values for these parameters for the instrument during various stages of development are listed in Table 1. The initial version of the prototype (9-91) suffered from a low "effective" quantum efficiency of the micro-channel plate due to electronic interference from the copper-vapor laser. Electronic discrimination against this interference caused a significant loss of the fluorescence pulses reaching the counter. Improved shielding of the pre-amplifier reduced this interference, allowing the use of lower discriminator levels. Additional improvements of the subsequent version of the prototype (3-92) included the addition of a mirror opposite the detection optics (×1.7) and antireflection coatings on all of the detection optics (×1.5). These versions employed a 25-mm diameter, 8-nm-band-pass (full-width at half-maximum, FWHM), ~10% transmissive interference filter centered at 309 nm (Barr Associates). The latest version of the prototype (7-92) includes a 25-mm, diameter, 8-nm-band-pass (FWHM), 35% transmissive interference filter (Barr Associates).

As can be seen from equation (10), the sensitivity of LIF based OH detection is proportional to laser power. However the effective laser power is limited by saturation of the OH electronic transition, which occurs when the ground electronic state of OH becomes depleted due to absorption of the pump radiation. Once the electronic transition is saturated, the remaining photons per pulse from the pump laser do not yield any additional fluorescent signal. The detected fluorescence signal varies almost linearly with the average laser power in the White cell for a stable OH concentration, as shown in Figure 4.. The sensitivities in Table 1 are calculated based on an average laser power of 15 mW, and as shown Figure 4, saturation of the OH transition at this power is less than 20%.

Comparison of the ambient air spectrum with the reference cell spectrum of OH demonstrates the selectivity of the instrument. Figure 5 shows a spectrum of OH from converted ambient HO_2 after reagent NO addition, along with the reference OH spectrum. The $Q_1(3)$, $Q_{21}(3)$, and the $P_1(1)$ lines of OH are clearly shown in the ambient spectrum. This scan was taken with the 3-92 version of the prototype instrument. Figure 5b shows the same spectral region from produced in the laboratory using the calibration systems described below. Similar spectra for ambient OH in the summertime should be possible with the improved sensitivity of the 7-92 version.

Minimum Detectable OH

The sensitivity, C, and the background signal determine the minimum detectable OH, given by:

$$[OH]_{min} = \frac{S/N\sqrt{2 \cdot S_{bkg}}}{C\sqrt{time}} \qquad (11)$$

For version 9-91, the background signal was 10-15 cts sec^{-1} for a laser power of 15 mW, resulting in a calculated minimum detectable OH of 5×10^5 molecules cm^{-3} in nitrogen and 6.5×10^5 molecules cm^{-3} in air for a signal-to-noise ratio (S/N) of 2 and an averaging time of 30 sec. With an averaging time of 5 minutes, the minimum detectable OH is 2.1×10^5 molecules cm^{-3} in air. For version 3-92, the background was 30 cts sec^{-1} at 15 mW, resulting in a calculated value of 1×10^5 molecules cm^{-3} in 30 sec and 4.2×10^4 molecules cm^{-3} in 5 min and in air for $[OH]_{min}$ ($S/N = 2$). Of this background signal, 1-3

cts sec^{-1} is due solar scatter, and approximately 1 ct sec^{-1} is due to detector noise. The remaining background signal is proportional to laser power, and is probably due to "ringing" of Rayleigh and chamber scatter inside the sampling cell. At present, the background signal for the latest version is approximately 90 cts sec^{-1} at 15 mW, but careful baffling of the laser beam in the sampling chamber should reduce this signal by a factor of 2 to 5, giving an expected value for $[OH]_{min}$ in air of approximately 5×10^4 molecules cm^{-3} in 30 sec and 1.7×10^4 molecules cm^{-3} in 5 minutes ($S/N = 2$).

The dependence of the calculated sensitivity and minimum detectable OH concentration on the density of nitrogen inside the detection chamber is illustrated in Figure 6 for the prototype versions using 15 mW of laser power. The lifetime of the OH excited state (τ), the quenching of the fluorescence (Q), and the fraction of fluorescence collected by the fixed gate (f_{gate}), all have a strong dependence on the pressure inside the detection chamber. As mentioned above, these effects roughly cancel the decrease in OH concentration upon expansion into the cell at the low pressures (ρ_{in}/ρ_{amb}). As a result, the calculated sensitivity and the minimum detectable OH change by less than 30% for air densities between 0.002 and 0.01 atm (Figure 6d - 6e). Thus small changes in internal pressure have little effect on the overall sensitivity of the instrument. The sensitivity of the instrument in air is reduced by 30% due to quenching of the OH excited state by O_2. Changes in the water vapor content of the ambient air also affects the instrument sensitivity as much as 30% due to quenching of the excited state. Thus, measurements of ambient OH must be accompanied by measurements of ambient H_2O to determine the instrument calibration.

Calibration

The most important and difficult aspect of the low pressure LIF technique is the absolute calibration of the instrument. The difficulty lies in the problem of producing a known concentration of OH at atmospheric pressure. For the low-pressure LIF technique, the problem can separated into internal and external calibrations, with the ratio reflecting the transmission of OH through the sampling inlet. The internal calibration can be accomplished using well established discharge-flow techniques for the production of known quantities of OH at pressures less than 5 torr [*Howard*, 1979; *Brune et al.*, 1983]. For the external calibration, OH is produced at atmospheric pressure from the photolysis of water vapor in two different systems. The first system produces OH concentrations on the order of ambient levels, and are calculated from the rate of water vapor photolysis. The second system produces OH concentrations which are high enough to be measured by UV absorption directly above the inlet.

To calibrate the internal detection axis, a 2.5-cm I.D., 66-cm long flow tube is inserted into the sampling chamber, just above the detection axis. This configuration is a resonable representation of the airflow distribution from the nozzle at the detection axis (Figure 3). OH radicals in this system are produced by titrating known concentrations of NO_2 with an excess of H atoms using the fast $H + NO_2 \rightarrow OH + NO$ reaction ($k_{298} = 1.3 \times 10^{-10}$ cm^3 $molecule^{-1}$ sec^{-1}) [*DeMore et al.*, 1992]. H atoms are produced using a microwave discharge of trace H_2 in a flow of He using a phosphoric acid quartz tube, or thermal dissociation of trace H_2 in He on a tungsten filament. NO_2 is added to the system through a movable injector. The position of the NO_2 injector is adjusted to maximize the production of OH, and to minimize the loss of OH due to the $OH + NO \rightarrow HONO$ reaction.

The internal calibrations were performed in 2-3 torr of N_2. Air was not used because of complications in the titration scheme resulting from the reaction of H atoms with O_2 (reaction 3b). NO_2 concentrations were varied from less than 1×10^8 to 2×10^9 cm^{-3}, while H concentrations were maintained at approximately $1 - 2 \times 10^{11}$ cm^{-3}. Because of high background signals due to the production of OH impurity from the microwave discharge, average laser power for these calibrations were less than 1 mW. The uncertainty associated with these calibrations is ±30%.

The external calibration of the instrument employed two different techniques. The first technique involves the production OH from the photolysis of a known amount of water vapor with a known flux of 185 nm radiation from a mercury lamp in a known amount of time:

$$H_2O + h\nu(< 246nm) \rightarrow OH + H \qquad (12)$$

OH concentrations are produced in the external flow system according to the photolysis equation

$$[OH] = [H_2O] \cdot \sigma_{H_2O} \cdot F_{185} \cdot \Delta t \qquad (13)$$

where $[H_2O]$ is the water vapor concentration in the flow system, measured using a chilled mirror hygrometer (General Eastern), σ_{H_2O} is the absorption cross

section of water vapor at 185 nm (5.5×10^{-20} cm^2) [*DeMore et al.*, 1992, F_{185} is the photon flux at 185 nm, and Δt is the photolysis exposure time (0.02-0.03 sec).

A 20-cm long, 7.5-cm I.D. flow tube is placed above the inlet to the LIF sampling chamber. Approximately 500-600 STD cm^3 sec^{-1} of N_2 is bubbled through distilled H_2O before entering the flow tube. Nitrogen, from liquid boil-off, was used instead of air to reduce the amount of reactive impurities in the system. The fraction of flow not captured by the inlet is vented through a screen below the nozzle. To produce a laminar airflow, the gas passes through a cluster of 8 100 x 100-mesh wire cloth and a set of 3-mm-I.D., 25-mm long flow straighteners. The photolysis source, located 2-5 cm above the inlet, consists of an 2.5-cm Hg lamp (Oriel) positioned end-on outside the flow tube. UV radiation is passed through a 25-mm diameter, 100-mm-f.l. lens and baffled by 2.5-cm by 1-cm rectangular mask, creating sheet of radiation across the airflow. The UV flux at 185 nm is measured using either a Hamamatsu R1187 phototube, or an absolutely calibrated EMR 541G photomultiplier tube. The EMR tube was calibrated at the Calibration Test Facility in the Physics Department at Johns Hopkins University against a photodiode that was recently calibrated at NIST. OH concentrations between 1×10^7 and 2×10^8 moleules cm^{-3} were produced in this system and were varied by changing the water vapor fraction in the main N_2 flow. Laser power for these calibrations were between 1 to 15 mW. To insure that the OH production was due solely to 185 nm photolysis of H_2O, a ~20% bandpass filter, centered at 186 nm (Acton Research) was placed in front of the UV source for some calibrations.

A crucial aspect of this calibration technique is the removal of reactive impurities from the system in order to insure that the OH concentration calculated from equation (13) does not change significantly before entering the LIF detection region. Purified N_2, from liquid boil-off, was passed through approximately 500 gm of dried Hopcalite (Callery) to reduce impurity CO to less than 1 ppbv. To insure that reactive loss of OH was minimal, the distance between the photolysis source and the inlet was varied, resulting in OH concentration changes of less than 15%. The purity of the system was also monitored by measuring the HO_2 concentration produced by the photolysis source. Photolysis of water vapor from reaction (12) produces one H atom for every OH molecule. The H atoms are converted to HO_2 through reaction (3b) ($k_\infty = 7.5 \times 10^{-11}$ cm^3 molecule^{-1} sec^{-1} [*DeMore et al.*, 1992]) in the prescence of a small amount of O_2 ($> 10^{14}$ cm^{-3}) in the system. In the absence of impurities which convert OH to HO_2, such as CO and hydrocarbons, this photolytic source produces HO_2 to OH concentration ratios of 1 or less. Assuming the absense of chemical loss during calibrations when [OH]=[HO_2], the uncertainty associated with the calculated OH concentrations at the present time is ±50%. This reflects the uncertainty associated with the radial distribution of the both the gas velocity in the source and the UV flux crossing the airstream.

The second external calibration technique eliminates the problem of reactive impurities in the system by measuring the absolute concentration of OH using absorption of UV radiation just above the inlet to the LIF sampling chamber. The disadvantage of this technique is that the small cross section of OH requires concentrations over 1000 times greater than ambient levels in order to measure the absorption over a short path length. However, this absorption external calibration technique together with the above photolysis technique establishes the linearity of the instrument sensitivity over a wide dynamic range.

A 30.5-cm long, 10-cm wide absorption cell, 25-cm high, is placed above the inlet to the LIF sampling chamber. A set of 8 100 x 100-mesh wire cloth and a set of ~3-cm diameter, 5-cm long hexcell flow straighteners establish a laminar profile of a > 1 STD liter sec^{-1} flow of N_2 and H_2O, purified as before. Nitrogen was used instead of air so that these external calibrations could be directly compared to the results of the photolysis calibration technique. Two 12.7-cm long Hg lamps (BHK), placed end-to-end along the length of the absorption cell, provide a uniform field of UV radiation 5-cm above the inlet to the sampling chamber. A small fraction of the UV laser radiation is diverted before entering the LIF detection chamber, and is directed into a White cell located directly above the inlet. The beam crosses the length of the absorption cell 40 times, resulting in an effective path length of 1000 cm. The UV beam is detected at the exit of the White cell using a photodiode.

Absolute OH concentrations are determined from the intensity of the UV beam using Beer's law

$$[\mathrm{OH}] = \ln\left(\frac{I_o}{I}\right) \cdot \sigma^{-1} \cdot L^{-1} \cdot \left(\frac{n_j}{n_o}\right)^{-1} \qquad (14)$$

where I_o/I is the ratio of the reference intensity of the laser to the absorbed intensity using the $Q_1(3)$ OH line, σ is the integrated absorption cross section

for OH (2.4×10^{-15} cm^2), L is the effective path length in cm, and n_j/n_o is the fraction of OH molecules in the rotational level where the absorption transition originates (0.075 for the $Q_1(3)$ branch at 298 K). OH concentrations as high as 1×10^{12} cm^{-3} were produced in this system.

To insure the uniformity of the OH concentration profile along the absorption axis, the entire cell was moved along the axis relative to the inlet, resulting in OH concentration variations of less than 10%. The OH concentration was varied over a limited range ($\sim 2\times10^{11} - 1\times10^{12}$ cm^{-3}) by changing the water vapor fraction in the main N_2 flow. Detection of OH concentrations less than 2×10^{11} cm^{-3} was limited by laser noise. The total laser power entering the LIF detection cell was reduced to less than 0.005 mW to maintain reasonable signal levels at these high OH concentrations. The photodiode was linear with laser power from 0.005 mW to 3 mW as determined by inserting neutral density filters into the beam. At these low laser powers and high OH concentrations, non-linearity of the MCP detector was approximately 20%. The uncertainty associated with this absorption calibration at the present time is ±50%, reflecting the uncertainty associated with the measurement of the laser power and the measured absorption signal.

Results of the calibrations of the prototype versions are summarized in Table 2. Internal calibrations were performed on the earliest versions of the prototype, while external calibrations were performed with the latest two versions. The values for the external calibrations incorporate both the photolysis and the absorption techniques. These are illustrated in Figure 7 for the 7-92 version. Calibrations based on the two different external calibration techniques agree to within 50%. The large variations in the observed calibration below 1×10^8 cm^{-3} of OH reflect the uncertainty associated with the water vapor concentration measurement as the H_2O concentration approaches the detection limit of the instrument. The sensitivities and minimum detectable OH in nitrogen for these versions using 15mW of laser power are compared to the calculated sensitivities in Figure 6e. The ~ 45% difference between the external and internal calibrations for the 3-92 version is mainly due to the different quenching environments for each calibration. The external calibrations reflect the sensitivity of the system under high concentrations of water vapor (~ 2%) and thus are in better agreement with the calculated sensitivities for nitrogen with 2% water vapor. The internal calibrations are performed under dry conditions. As can be seen from Figure 6e and Table 2, the expected and calibrated sensitivities agree to within 40%.

The internal calibration for the 3-92 version of the instrument is 20% higher than the external calibration, but are within the 50% uncertainty in the external calibration methods. Given the large uncertainty presently associated with the external calibrations, small losses of OH on the inlet are difficult to quantify, and are not constrained to better than 50%. However, different inlet designs (flat and conical) and surfaces (bare aluminum, Teflon and Halocarbon wax coatings) gave the same OH signal to within 20%. This insensitivity of the instrument's performance to the shape of the nozzle as well as the coating of the external surfaces imply that heterogeneous loss is not occuring near the throat of the inlet. This is not surprising given the rapid velocity of the airstream at the throat of the nozzle. However, resolution of this issue requires further work.

The instrument sensitivity was monitored in the field by continuous measurements of laser power at the exit of the White cell. The laser power is the most likely term in equation (10) to exhibit large fluctuations in the field, but certainly not the only variable that may change. Presently, the instrument sensitivity is also monitored in the field by periodic measurements of Rayleigh scatter, made by allowing the detection cell to fill with the dry N_2 or Ar confining flow. The ratio of OH detection sensitivity and Rayleigh and Raman scattering detection sensitivity is given by:

$$\frac{C_{OH}}{C_R} \sim \frac{\sigma_0}{\sigma_{Ray}}\left(\frac{4\ln 2}{\pi}\right)^{1/2}\cdot\left(\Delta\nu_L^2+\Delta\nu_D^2\right)^{-1/2}\cdot\left(\frac{\Delta N}{N}\right)\cdot Q\cdot\frac{f_{gate}}{f_{pol}} \qquad (15)$$

σ_0 and σ_{Ray}	scattering cross sections by OH and air.
$\Delta\nu_D$ and $\Delta\nu_l$	OH Doppler and the laser line widths, repectively.
$\Delta N/N$	fraction of OH molecules in the rotational level being excited.
Q	quenching of the OH excited state.
f_{gate}	fraction of the OH fluorescence collected.
f_{pol}	fraction of the polarized Rayleigh scattering measured.

Variations in the optical geometry, collection efficiency and laser power which affect the OH detection sensitivity is reflected by changes in the observed

Rayleigh scatter signal. For a given temperature and pressure, $\Delta N/N$ is fixed and Q can be calculated and verified through measurements. The stability of f_{gate} and $\Delta\nu_L$ can also be determined. Thus sensitivity of the instrument to scattering, combined with laboratory measurements of the relationship of scattering to OH sensitivity, reflects the absolute calibration of the instrument. At present, changes in the calibration from day to day are due to laser power fluctuations. However, long term variations in the calibration due to other variables and different quenching environments will determined as the calibration history improves.

The conversion efficiency of HO_2 to OH was determined using a simple titration technique employing the photolytic OH calibration system described above. OH produced in the source is first converted externally to HO_2 by adding a small flow of a 12 ppm mixture of CO in N_2 (Matheson) ([CO] $\sim 1\times10^{13}$ cm^{-3}). This converts the external OH to HO_2 through reactions (3a) and (3b). The HO_2 is then converted back to OH inside the chamber through NO addition through the loop injector. Assuming that any losses upon expansion into the sampling chamber are similar for both OH and HO_2, changes in the total HO_x signal (OH + HO_2) due to external CO addition simply reflects the conversion efficiency of HO_2 to OH. This simple experiment eliminates a number of uncertainties associated with other HO_2 calibration methods involving the measurement of the decay of HO_2 due to self reaction in an external reactor [*Hard et al.*, 1992a]. The efficiency of the 9-91 version was only 7% due to insufficient reaction time, and poor mixing of the NO with the internal airstream. For the 3-92 and the 7-92 versions of the prototype, this efficiency was improved to 93±5% by increasing the overall reaction time with NO, and by decreasing the size of the loop injector, allowing for more efficient mixing with the airstream. This efficiency is comparable to kinetic simulations of the system, which indicate a conversion efficiency of greater than 95%, as seen in Figure 8. The falloff of the observed OH signal in Figure 8 is primarily due to the loss of OH from the OH + NO + M→ HONO + M reaction (k_o = 7 × 10^{-31} cm^6 molecule^{-2} sec^{-1}), which becomes important at long reaction times or high NO concentrations. The NO concentration is routinely varied to ensure that HO_2 + NO titration is complete without overtitrating.

The OH signal produced from addition of NO to the ambient airstream is due to HO_2 rather than RO_2, as computer simulations of the kinetics indicate (Figure 8). RO_2 is converted to HO_2 in the presence of NO and O_2 through reactions (7) and (8). Although the conversion of RO_2 to RO by NO is rapid in this system, the short reaction time and low air density prevents the rapid conversion of RO to HO_2. As shown in Figure 8, when [RO_2]=[HO_2], less than 2% of the observed converted OH signal is due to ambient RO_2. More quantitative tests are still required to verify this interference.

Interferences

As mentioned above, laser-generated OH has been the most serious interference of previous LIF techniques to measure tropospheric OH. This interference is substantially reduced in the present system due to the laser excitation technique and the low pressure sampling of ambient air. To test the system for the production of OH by the laser, 300 ppbv of ozone and 3% water vapor were added to a flow of air in the laboratory. Under these extreme conditions, the resulting OH signal was only 2 ± 2 counts sec^{-1} ($\sim 10^5$ OH cm^{-3}) with a laser power of 25 mW at 308 nm using version 3-92 of the prototype. This laser power is almost a factor of 2 greater than the maximum laser power used in field measurements. Thus, interferences due to laser-generated OH is insignificant in this system.

The other significant interference mentioned above is the broad-band fluorescence of other species excited by the laser radiation. Atmospheric abundances of hydrogen peroxide produced in the laboratory does not produce a significant background signal in this instrument (< 2 counts sec^{-1}). Potential interfences from other molecules, such as SO_2 and CH_2O will be tested as part of future calibration measurements. As discussed below, the background signal measured in the atmosphere is the same as it is in the laboratory using dry N_2 as the source gas. This implies that broad-band fluorescence of organic molecules or aerosols does not contribute significantly to the instrument background signal.

Results and Discussion

The early versions of the prototype were used to measure ambient OH and HO_2 from the roof of the Walker building on the Penn State campus which is located adjacent to a busy downtown street. Figure 9 shows the signal levels for OH and HO_2 taken on September 17, 1991 with the 9-91 version of the prototype instrument. In this figure, the solid line is

the observed signal in counts sec^{-1} from ambient air, while the dotted line is the OH signal from the reference cell, indicating when the dye laser is tuned into resonance with the $Q_1(3)$ transition at 308.24 nm. The larger signals in the figure are the result of NO addition to the ambient airstream and thus represent HO_2 abundances. Data is collected every second, and is displayed as 10-sec averages in the top panel, and 30-sec averages in the second panel to improve the signal-to-noise level.

The vertical scale has been expanded in the second panel of Figure 9 to emphasize the signal due to ambient OH. The on-resonance signal due to ambient OH of $\sim$10 counts sec^{-1} is clearly seen above the off-resonance background signal of $\sim$ 16 counts sec^{-1}. This background is primarily due to laser scattering in the detection cell, as indicated from the correlation of the variation of the laser power in the bottom panel with the off-resonance signal. The magnitide of the background signal was independent of the ambient conditions and was identical to background signals measured in the laboratory. There are two cases in Figure 9, at 3:35-3:37 and 3:51-3:53, where the OH signal decreases even though the laser remained tuned on resonance with the OH transition. In these cases, denoted by "C_3F_6" in the figure, perfluoropropylene (CF_3CFCF_2, Matheson, 99.5%) was added through the loop injector to remove ambient OH from the airstream through the fast OH + $C_3F_6 \rightarrow$ adduct reaction ($k_{298} = 2 \times 10^{-12}$ cm^3 $molecule^{-1}$ sec^{-1} [P. Wennberg, unpublished data, 1991; *McIlroy and Tully*, 1993]. This "chemical modulation" of the OH signal serves as a test for the contribution of laser-generated OH to the observed signal. OH produced in the path of the White cell does not have sufficient time to react with C_3F_6 before detection, and a signal due to this interference would remain above the off-resonance background signal. Perfluoropropylene is used as the chemical modulator because it does not contain hydrogen atoms which, in addition to H_2O, could serve as a source of laser-generated OH. Because the chemical and spectral backgrounds in Figure 9 are the same, interference due to laser-generated OH is small, and the observed signal is due solely to ambient OH.

Figure 10 shows a 30-minute segment of data taken on September 17, 1991. The top panel shows the ambient and reference cell signals averaged over 10 seconds. The on-resonance signal of $\sim$5-6 counts sec^{-1} can still be seen above the off-resonance background signal even though the laser power during this segment was 33% lower than that for Figure 9. The second panel in this figure shows both the UV solar flux (filled circles, measured using a silicon photodiode equipped with a UG-11 visible filter) as well as the total solar flux (open circles). Small variations in the OH signal appears to correspond with variations in the solar UV flux and O_3 around 12:20-12:22. The gradual drop of the on-resonance signal after 12:24 corresponds to the drop in the solar UV, which remains low as the total solar flux changes due to variations in the cloud cover. The rough correlation of the observed OH signal with variations in photochemical sources for OH suggest that variations in the observed signal are not due to instrument artifacts.

Assuming that loss of ambient OH on the inlet is small (based on the 3-92 internal and external calibrations) the instrument sensitivity constant, C, was $(2.4 \pm 1.2) \times 10^{-6}$ (counts sec^{-1})/(molecule cm^{-3}) using the 9-91 internal calibration adjusted to account for the increased quenching of the OH excited state in air. Figure 11 shows the diurnal trend for OH and HO_2 for Septermber 17, 1991 displayed as 5-minute averages. As can be seen from this figure, midday levels of OH were were highly variable due to cloudy conditions, with a slow decline under clear skies in the afternoon, under relatively clean conditions. Ozone mixing ratios were highly variable and averaged about 60 ppbv, and water vapor was 1600 ppmv. The 1σ statistical uncertainty in these measurements of OH and HO_2 is $\pm$30% of the peak values, while the absolute uncertainty is $\pm$50% due to the uncertainty associated with the absolute calibrations mentioned above.

Periodic measurements of HO_2 by the addition of NO are also shown in Figure 11. Because of poor mixing and the limited reaction time for the 9-91 version, the conversion efficiency for these measurements was only about 20%. Because of this low conversion efficiency, the uncertainty in the HO_2 concentrations is larger for these measurements than that for the OH measurements. The conversion efficiency was improved to 93% by reducing the loop diameter of the injector, thus increasing the mixing of NO with the ambient airstream. In addition, the reaction time was increased by increasing the distance between the loop injector and the detection axis. With these improvements, HO_2 can now be detected with the same uncertainty as for OH.

Measurements were made with the improved 3-92 version on March 18, 1992 on the roof of the Walker building under cloudy, winter conditions. Ozone mixing ratios were approximately 35 ppbv, and water va-

por was 3000 ppmv. The laser power for these measurements was less than optimum, averaging about 7-8 mW over the course of the day. Based on the internal and external calibrations for this version, the instrument sensitivity constant on this day was $(7.3 \pm 0.5) \times 10^{-6}$ (counts sec^{-1})/(molecule cm^{-3}), adjusted to account for the increased quenching of the OH fluorescence in air. The improved sensitivity of the instrument is shown in Figure 12, where the signal due to ambient OH and HO_2 is displayed as 4-sec averages. Addition of C_3F_6, as shown in the figure, resulted in chemical background signals which agreed well with the off-resonance background. The signal-to-noise ratio for OH was 12 in 30 seconds, and 36 in 1 second for HO_2.

Figure 13 shows the OH and HO_2 data for the March 18, 1992 measurements. The frequency of data is not representive of the capability of the instrument, as measurements were interrupted to allow for configuation tests of the flow and HO_2 conversion efficiency. Early morning concentrations of OH were only $3 - 4 \times 10^5$ molecules cm^{-3}, near the detection limit of the instrument. A frontal passage in the afternoon coincided with a sudden rise in OH and HO_2. During this episode, cloud cover decreased the total solar flux by a factor of 2, ozone increased by 5 ppbv, and water vapor varied from 1500 ppmv to 3000 ppmv. OH concentrations peaked at $(2.2 \pm 1.0) \times 10^6$ molecules cm^{-3} in the afternoon, before falling off to less than 7×10^5 molecules cm^{-3}, 2-3 hours after the frontal passage. HO_2 abundances were approximately $(6 \pm 1) \times 10^7$ molecules cm^{-3} during this episode. Clearly there were not enough measurements of other important species to estimate the expected OH concentration during this episode, but the rough correlation of OH with O_3 and H_2O suggests that the sudden rise in OH concentration was due to the passage of an airmass in a different photochemical equilibrium over the instrument.

Conclusions

Although previous attempts to measure tropospheric OH by laser-induced fluorescence have suffered from uncertainties associated with a number of interferences generated by the technique itself, the prototype instrument described above has been designed to minimize these interferences. Specifically, exciting and detecting OH in the $A^2\Sigma^+ v' = 0 \rightarrow X^2\Pi v'' = 0$ band near 308 nm using a high repetition-rate laser system reduces interference from laser-generated OH to negligible levels, as well as eliminating broad-band fluorescence from other ambient species. The incorporation of a fast-switching microchannel plate detector allows temporal gating of the Rayleigh scatter associated with the laser pulse, which avoids the high noise levels associated with transient saturation of photomultiplier tubes. HO_2 can be detected with the same sensitivity as OH by the addition of NO to the ambient airflow. Because of the reduction in pressure, conversion of ambient RO_2 to OH resulting from NO addition is small.

This instrument has the advantages of both sensitivity and selectivity in the measurement of tropospheric OH and HO_2. Although it is clear that sensitive measurements of ambient OH and HO_2 can be made with this instrument, the absolute calibration of this instrument still requires some improvement, and additional potential interferences need to be investigated. The largest uncertainty associated with the present instrument is in the absolute calibration of the inlet transmission of OH and HO_2. Although the present calibrations indicate insignficant losses of OH and HO_2 on the inlet, they still require some improvement in order to decrease the present uncertainty of $\pm 50\%$. In addition to inlet loss, the effect of cooling of the jet on homogeneous reaction rates in the cell, as well as the effect of adduct formation in the cooled jet expansion needs to be addressed; specifically the $HO_2 \cdot H_2O$ complex, which may affect the disproportionation of HO_2 and OH. The effect of adduct formation involving HO_2 in this instrument seems unlikely given the high calibrated conversion efficiency of HO_2 to OH. Also, the effect of the instrument sensitivity with varying ambient conditions, such as different trace gas concentrations, wind speed and direction across the nozzle and temperature needs to be studied in further detail as part of future calibration measurements.

Future improvements to the calibration techniques will include a redesigned UV source for the photolytic calibration which will increase the production of OH, remove the uncertainty associated with the flux distribution, and allow variations in the total flux, thus producing variable OH concentrations under constant concentrations of water vapor. External calibrations will then be performed under both "wet" and "dry" conditions, allowing more direct comparisons to internal calibrations under similar quenching conditions. Reduction of the power fluctuations associated with the UV laser beam should allow the absorption technique to measure OH concentrations down to less

than 10^{11} cm^{-3}. These improvements should reduce the uncertainty in both techniques to less than 20%, and effectively increase the precision of the overall calibration by overlapping the OH concentration range covered by each method. External calibrations will also be performed in air rather than nitrogen, resulting in a more accurate calibration of the instrument under ambient quenching conditions. Various trace gases, such as SO_2 and CH_2O, will be added to the external flow to determine any potential fluorescent interference with the detection of ambient OH. Also, the effect of air motion across the nozzle on the transmission of OH through the inlet will be examined during field measurements by studying possible correlations of the detected OH signal with wind speed and direction. These tests and improvements should further quantify the various potential effects of inlet sampling and ambient interferences on the instrument sensitivity.

The minimum detectable OH and HO_2 for this instrument of less than 1×10^5 molecules cm^{-3} in 30 seconds is sufficient for measurement throughout the troposphere. In conjunction with measurements of CO, NO_x, water vapor, ozone and other species, the fast measurements of OH and HO_2 by this instrument is capable of providing a true test of photochemical models of the troposphere.

Acknowledgments We would like to thank C. Fong for experimental assistance, R. Pelton for calibration of our photomultiplier tube, and P. Wennberg, A. Hofzumahaus, F. Eisele and G. Mount for helpful discussions. We would also like to thank D. Crosley for helpful comments on the manuscript. This work was supported by the National Science Foundation (grant ATM-8909155) and NASA (grant NAG-1-1057).

References

Anderson, J. G., The absolute concentration of OH ($X^2\Pi$) in the earth's stratosphere, *Geophys. Res. Lett., 3*, 165, 1976.

Armerding, W., A. Herbert, M. Spiekermann, J. Walter, and F. J. Comes, Fast scanning laser DOAS - A very promising technique for monitoring OH and other tropospheric trace gases, *Fresenius J. Anal. Chem., 340*, 654, 1991.

Bradshaw, J. D., M. O. Rogers, and D. D. Davis, Sequential two-photon laser-induced fluorescence: A new technique for detecting hydroxyl radicals, *Appl. Opt., 23*, 2134, 1984.

Brune, W. H., J. J. Schwab, and J. G. Anderson, Laser magnetic resonance, resonance fluorescence, and resonance absorption of the reaction kinetics of $O + OH \rightarrow H + O_2$, $O + HO_2 \rightarrow OH + O_2$, $N + OH \rightarrow H + NO$, and $N + HO_2 \rightarrow$ products at 300 K between 1 and 5 torr, *J. Phys. Chem., 87*, 4503, 1983.

Cantrell, C. A., D. H. Stedman, and G. J. Wendel, Measurement of atmospheric peroxy radicals by chemical amplification, *Anal. Chem., 56*, 1496, 1984.

Chan, C. Y., T. M. Hard, A. A. Mehrabzadeh, L. A. George, and R. J. O'Brien, Third-generation FAGE instrument for tropospheric hydroxyl measurement, *J. Geophys. Res., 95*, 18,569, 1990.

Cleveland, C. B., and J. R. Wiesenfeld, Electronic quenching of highly rotationally excited OH ($A^2\Sigma^+$, v'= 0, 1) by H_2O, *Chem. Phys. Lett., 144*, 479, 1988.

Copeland, R.A., and D.R. Crosley, Temperature dependent electronic quenching of OH ($A^2\Sigma^+, v' = 0$) between 230 and 310 K, *J. Chem. Phys., 84*, 3099, 1986.

Crosley, D. R., Local measurement of tropospheric HO_x, *NASA Conf. Publ.*, to be published, 1993.

Crutzen, P., A discussion of the chemistry of some minor constituents in the stratosphere and the troposphere, *Pure Appl. Geophys., 106*, 1385, 1973.

Crutzen, P., Photochemical reactions initiated by and influencing ozone in unpolluted tropospheric air, *Tellus, 26*, 47, 1974.

Davis, D. D., W. Heaps, and T. McGee, Direct measurements of natural tropospheric levels of OH via an aircraft borne tunable dye laser, *Geophys. Res. Lett., 3*, 331, 1976.

Davis, D. D., M. O. Rogers, S. D. Fischer, and K. Asai, An experimental assessment of the O_3/H_2O interference problem in the detection of natural levels of OH via laser induced fluorescence, *Geophys. Res. Lett., 8*, 69, 1981a.

Davis, D. D., M. O. Rogers, S. D. Fischer, and W. S. Heaps, A theoretical assessment of the O_3/H_2O interference problem in the detection of natural levels of OH via laser induced fluorescence, *Geophys. Res. Lett., 8*, 73, 1981b.

DeMore, W. B., S. P. Sander, D. M. Golden, R. F. Hampson, M. J. Kurylo, C. J. Howard, A. R. Ravishankara, C. E. Kolb, and M. J. Molina, Chemical

kinetics and photochemical data for use in stratospheric modeling, *JPL Publ. 92-20*, 1992.

Dimpfle, W. L., and J. L. Kinsey, Radiative lifetimes of OH ($A^2\Sigma$) and Einstein coefficients for the A-X system of OH and OD, *J. Quant. Radiat. Transfer, 24*, 233, 1979.

Dorn, H. P., J. Callies, U. Platt, and D. H. Ehhalt, Measurement of tropospheric OH concentrations by laser long-path absorption spectroscopy, *Tellus, 40(B)*, 437, 1988.

Eisele, F. L., and D. J. Tanner, Ion-assisted tropospheric OH measurements, *J. Geophys. Res., 96*, 9295, 1991.

Felton, C. C., J. C. Sheppard, and M. J. Campbell, The radiochemical hydroxyl radical measurement method, *Environ. Sci. Technol., 24*, 1841, 1987.

German, K. R., Radiative and predissociative lifetimes of the v'= 0, 1 and 2 levels of the $A^2\Sigma^+$ state of OH and OD, *J. Chem. Phys., 63*, 5252, 1975.

German, K. R., Collision and quenching cross sections in the $A^2\Sigma^+$ state of OH and OD, *J. Chem. Phys., 64*, 4065, 1976.

Hard, T. M., R. J. O'Brien, C. Y. Chan, and A. A. Mehrabzadeh, Tropospheric free radical determination by FAGE, *Environ. Sci. Technol., 18*, 768, 1984.

Hard, T. M., C. Y. Chan, A. A. Mehrabzadeh, W. H. Pan, and R. J. O'Brien, Diurnal cycle of tropospheric OH, *Nature, 322*, 617, 1986.

Hard, T. M., C. Y. Chan, A. A. Mehrabzadeh, and R. J. O'Brian, Diurnal HO_2 cycles at clean air and urban sites in the troposphere, *J. Geophys. Res., 97*, 9785, 1992a.

Hard, T. M., A. A. Mehrabzadeh, C. Y. Chan, and R. J. O'Brien, FAGE measurements of tropospheric HO with measurements and model of interferences, *J. Geophys. Res., 97*, 9795, 1992b.

Hastie, D. R., M. Weissenmayer, J. P. Burrows, and G. W. Harris, Calibrated chemical amplification for atmospheric RO_x measurements, *Anal. Chem., 63*, 2048, 1991.

Hofzumahaus, A., H.-P. Dorn, and U. Platt, Tropospheric OH radical measurement techniques: recent developments, in *Physico-chemical behavior of atmospheric pollutants*, edited by G. Restelli and G. Angeletti, pp. 103-108, Kluver, 1990.

Hofzumahaus, A., H.-P. Dorn, J. Callies, U. Platt, and D. H. Ehhalt, Tropospheric OH concentration measurements by laser long-path absorption spectroscopy, *Atmos. Environ., 25A*, 2017, 1991.

Howard, C. J., Kinetic measurements using flow tubes, *J. Phys. Chem., 83*, 3, 1979.

Levy, H., Normal atmosphere: Large radical and formaldehyde concentrations predicted, *Science, 173*, 141, 1971.

Logan, J. A., M. J. Prather, S. C. Wofsy, and M. B. McElroy, Tropospheric chemistry: A global perspective, *J. Geophys. Res., 86*, 7210, 1981.

McIlroy, A., and F. P. Tully, Kinetic study of OH reactions with perfluoropropene and perfluorobenzene, *J. Phys. Chem., 97*, 610, 1993.

Mihelcic, D., A. Volz-Thomas, H. W. Pätz, D. Kley, and M. Mihelcic, Numerical analysis of ESR spectra from atmospheric samples, *J. Atmos. Chem., 11*, 271, 1990.

Mount, G. H., The measurement of tropospheric OH by long path absorption 1. Instrumentation, *J. Geophys. Res., 97*, 2427, 1992.

Mount, G. H., and F. L. Eisele, An intercomparison of tropospheric OH measurements at Fritz Peak Obeservatory, Colorodo, *Science, 256*, 1187, 1992.

Nelson, D. D., and M. S. Zahniser, Diode laser spectroscopy of ν_3 vibration of HO_2, *J. Mol. Spec., 150*, 527, 1991.

O'Brien, R.J., and T.M. Hard, Tropospheric hydroxyl radical: A challenging analyte, *Adv. Chem. Ser. 232*, edited by L. Newman, p. 323, American Chemical Society, 1993.

Ortgies, G., K.-H. Gericke, and F. J. Comes, Is uv laser induced fluorescence a method to monitor tropospheric OH? *Geophys. Res. Lett., 7*, 905, 1980.

Perner, D., U. Platt, M. Trainer, G. Hübler, J. W. Drummond, D. H. Ehhalt, G. Helas, W. Junkermann, R. Rudolph, B. Schubert, K. J. Rumpel, and A. J. Voltz, Tropospheric OH concentrations: A comparison of field data with model predictions, *J. Atmos. Chem., 5*, 185, 1987.

Prinn, R., D. Cunnold, R. Rasmussen, P. Simmonds, F. Alyea, A. Crawford, P. Fraser, and R. Rosen, Atmospheric trends in methylchloroform and the global average for the hydroxyl radical, *Science, 238*, 945, 1987.

Shapiro, A.H., *The Dynamics and Thermodynamics of Compressible Fluid Flow, Parts I and II from*

Volume I, p. 83, The Ronald Press Company, New York, 1958.

Shirinzadeh, B., C. C. Wang, and D. Q. Deng, Diurnal variation of the OH concentration in ambient air, *Geophys. Res. Lett., 14*, 123, 1987.

Smith, G., and D. R. Crosley, A photochemical model of ozone interference effects in laser detection of tropospheric OH, *J. Geophys. Res., 95*, 16427, 1990.

Stimpfle, R. M., and J. G. Anderson, In-situ detection of OH in the lower stratosphere with a balloon borne high repetition rate laser system, *Geophys. Res. Lett., 15*, 1503, 1988.

Stimpfle, R. M., L. B. Lapson, P. O. Wennberg, and J. G. Anderson, Balloon borne in-situ detection of OH in the stratosphere from 37 to 23 km, *Geophys. Res. Lett., 16*, 1433, 1989.

Thompson, A. M., The oxidizing capacity of the earth's atmosphere: Probable past and future changes, *Science, 256*, 1157, 1992.

Trainer, M., E. Y. Hsie, S. A. McKeen, R. Tallamraju, D. D. Parrish, F. C. Fehsenfeld, and S. C. Liu, Impact of natural hydrocarbons on hydroxyl and peroxyl radicals at a remote site, *J. Geophys. Res., 92*, 11879, 1987.

Wang, C. C., L. I. Davis, C. H. Wu, and S. Japar, Laser-induced dissociation of ozone and resonance fluorescence of OH in ambient air, *Appl. Phys. Lett., 28*, 14, 1976.

Weinstock, B., Carbon Monoxide: Residence time in the atmosphere, *Science, 166*, 224, 1969.

Wysong, J.J., J.B. Jefferies, and D.R. Crosley,, Quenching of $A^2\Sigma^+$ OH at 300 K by several colliders, *J. Chem. Phys., 92*, 5218, 1990.

Table 1. Parameters for the OH sensitivity equation

	Prototype version		
	9-91	3-92	7-92
B_{12}(cm^3 J^{-1} s^{-2})	1.01×10^{24}		
$\Delta\nu_D$ (cm^{-1})	0.10		
$\Delta\nu_l$ (cm^{-1})	0.15		
$\Delta N/N$	0.075		
P (W)	0.015		
l (cm)	24.0		
ϵ	0.05	0.085	
η	0.015	0.036	
T	0.05	0.075	0.23
Q	0.33		
f_{gate}	0.55		
ρ_{in}/ρ_{amb}	0.0041		
C[a]	4.6	28	87

[a] 10^{-6} (cts sec^{-1}/(OH cm^{-3}))

Table 2. OH sensitivity calibration results

	Prototype version		
	9-91	3-92	7-92
Calculated (N_2)[a]	0.31	1.9	5.8
Internal	$0.23 \pm .08$	1.6 ± 0.5	
Calculated (2% H_2O)	0.25	1.5	4.6
External[b]		1.0	3.0
External[b,c]		0.8	2.0

[a] sensitivities in 10^{-6} (cts s^{-1} mW^{-1})/(OH cm^{-3})

[b] uncertainty factor = 1.5

[c] adjusted for air

This preprint was prepared with the AGU LaTeX macros v3.0. File instrl formatted 1994 January 3.

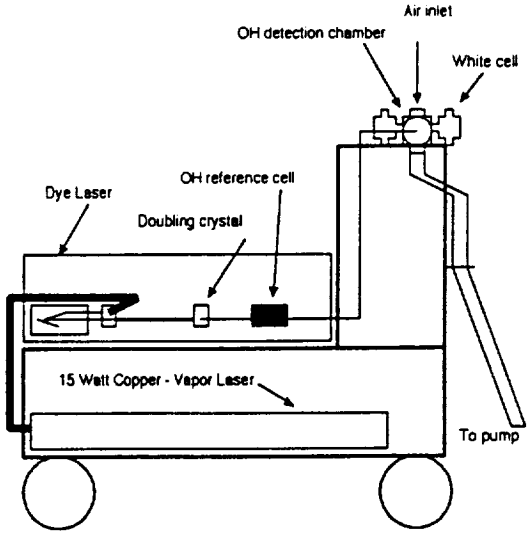

Figure 1. Schematic of the prototype OH/HO_2 instrument.

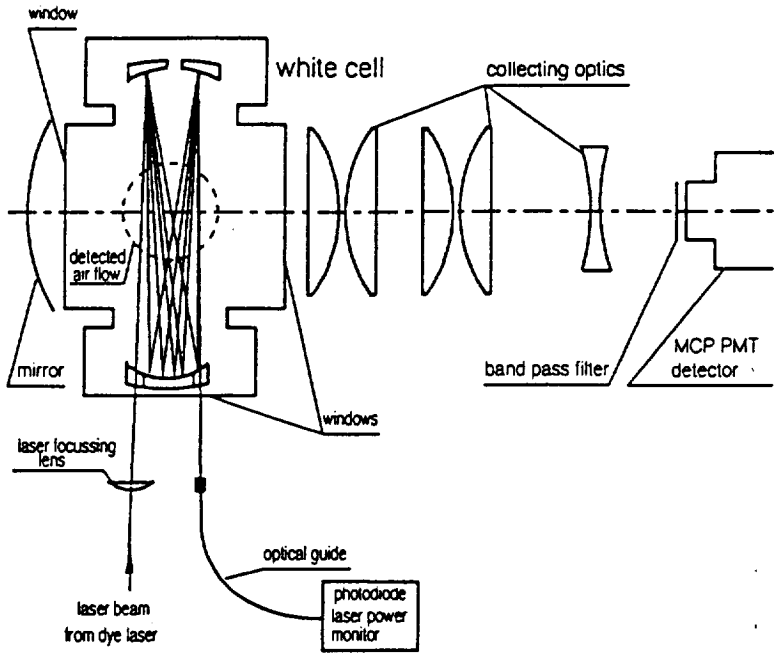

Figure 2. Optical layout of the OH/HO_2 instrument, including the White cell and the collecting optics leading to the microchannel plate detector (MCP PMT).

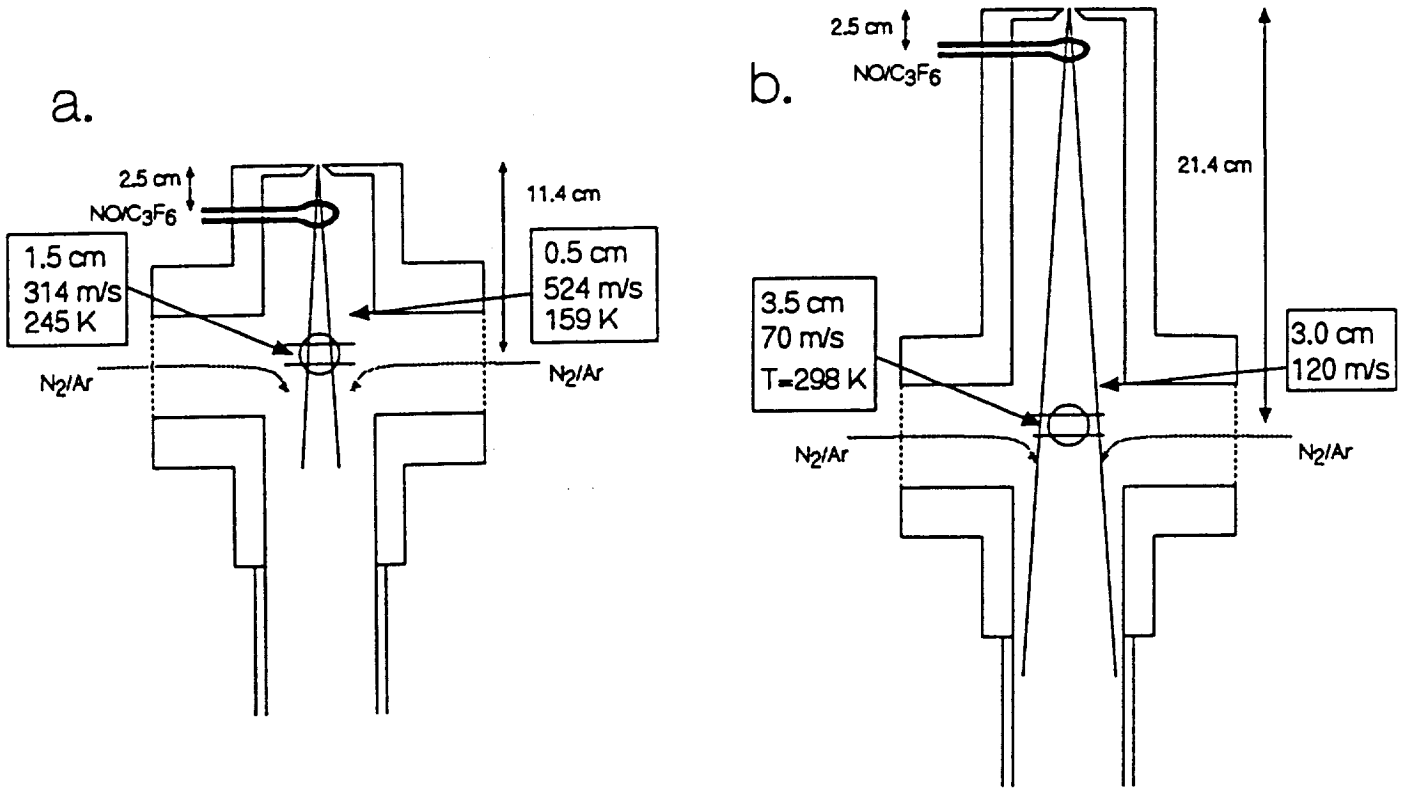

Figure 3. Schematic of the internal flow measured using a pitot tube for (a) the 9-91 prototype version, and (b) the 3-92 version (not to scale). Shown are the relative heights of the inlet and reagent injector above the detection volume. Values in boxes correspond to the jet diameter and velocities measured at the indicated points along the jet. Temperatures in a) are calculated from the velocity measurements, and in b) from fast thermister measurements (see text). Notice the overlap with the laser beam (two horozontal lines) and the detector field-of-view (circle). Small flows of nitrogen or argon added near the White cell mirrors help confine the airstream.

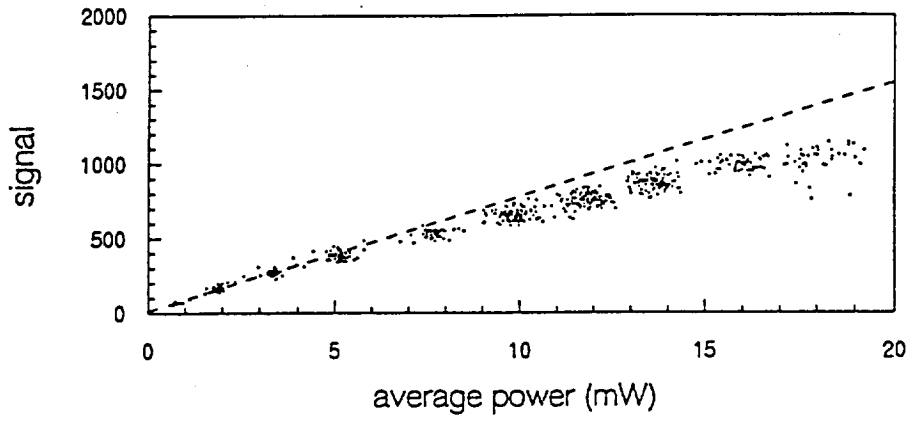

Figure 4. The measured OH signal plotted as a function of the average laser power in the White cell. The dashed line is a fit to the data when the laser power was less than 4 mW. Deviation of the measured signal from this fit shows the effect of saturation of the OH transition.

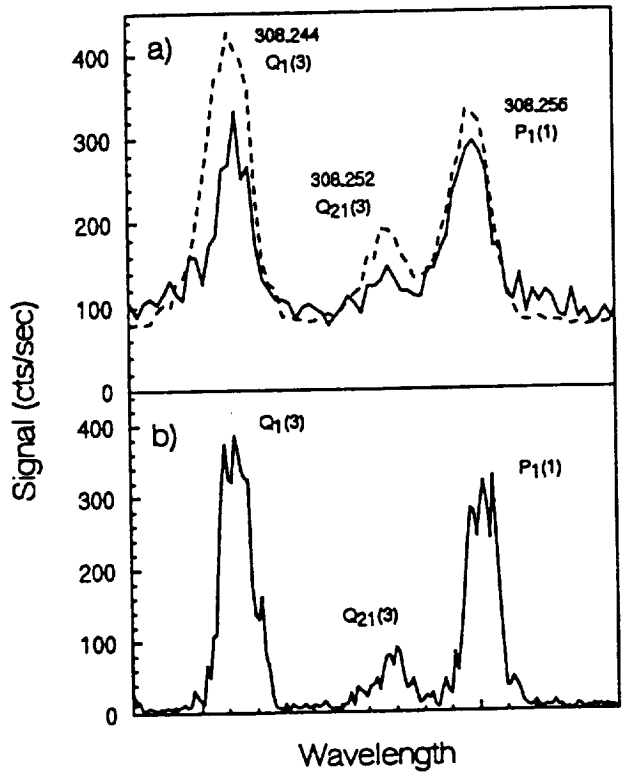

Figure 5. a) Spectrum of OH from partially converted ambient HO_2, recorded on June 25, 1992. The dotted line is the reference cell signal from thermal OH production. b) OH spectrum measured in the laboratory from external photolytic OH production. Wavelengths are given in nm.

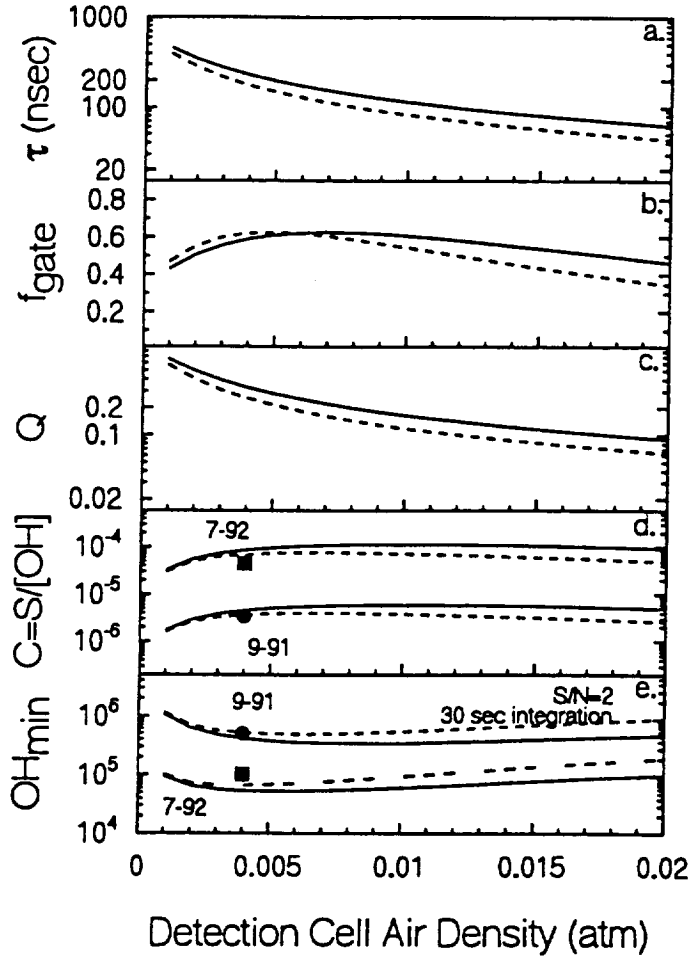

Figure 6. The effect of the total density in the detection chamber on (a) the OH lifetime; (b) the fraction of the fluorescence collected by the gated detector; (c) the quenching of the OH excited state; (d) the calculated instrument sensitivity; and (e) the calculated minimum detectable OH for 15 mW of laser power. The solid lines are for dry nitrogen and the dashed lines are for nitrogen with 2% water vapor. Filled points indicate experimental values.

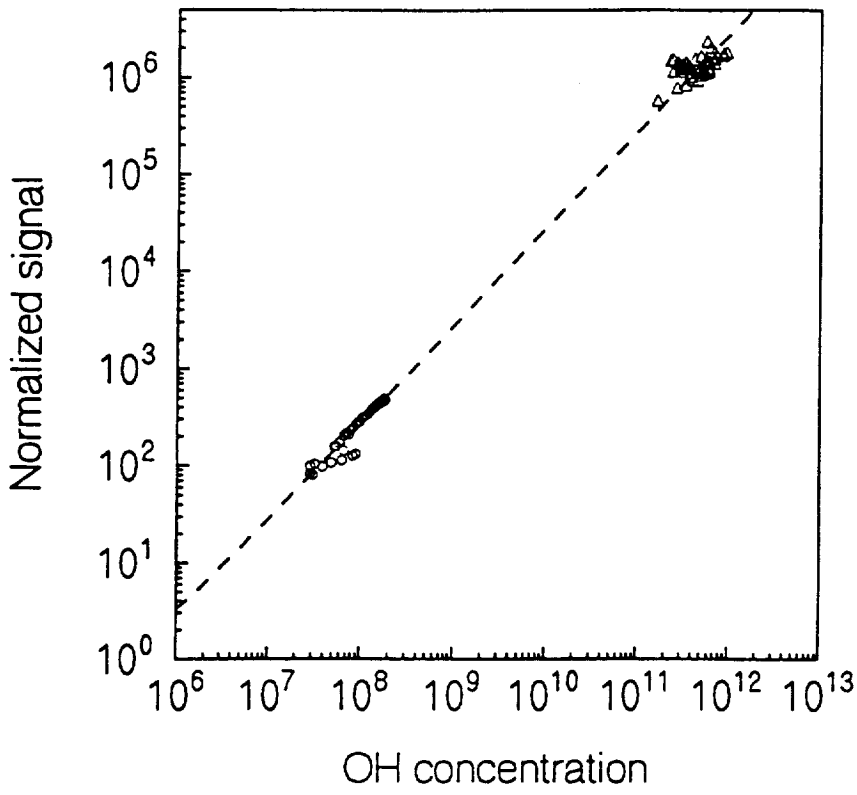

Figure 7. Log-log plot of the external OH concentration in nitrogen versus observed signal for the 7-92 prototype version. The signal is scaled to 1 mW of average laser power in the White cell. The circles are results from a single calibration using the photolysis cell technique at ~15 mW average laser power. The triangles are calibration results using the absorption cell technique at average an average laser power of less than 0.005 mW.

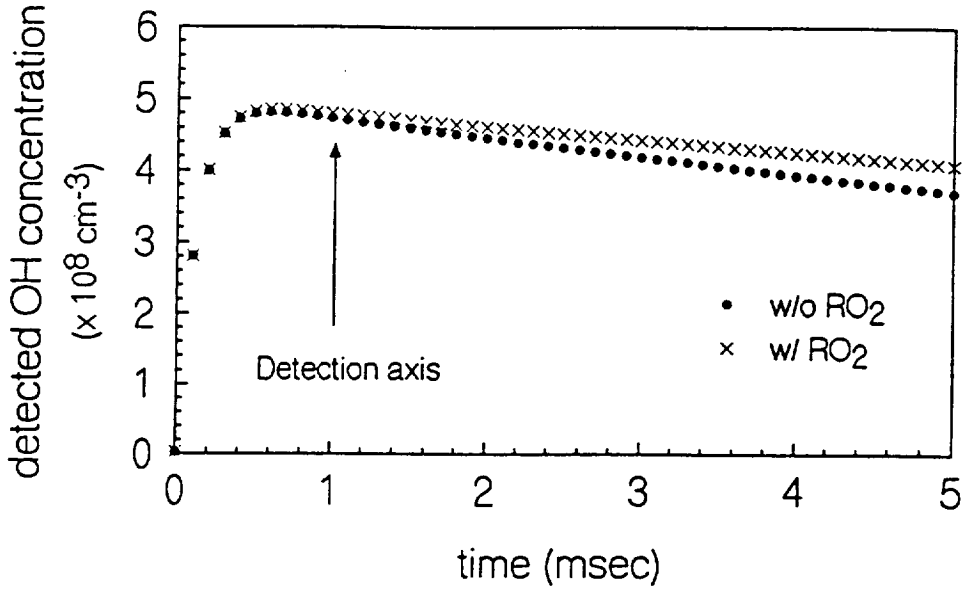

Figure 8. Simulation of the conversion of HO_2 and RO_2 to OH in the prototype instrument. The RO_2 abundance is assumed to be twice the HO_2 abundance. OH is detected approximately 1 msec after the addition point for NO.

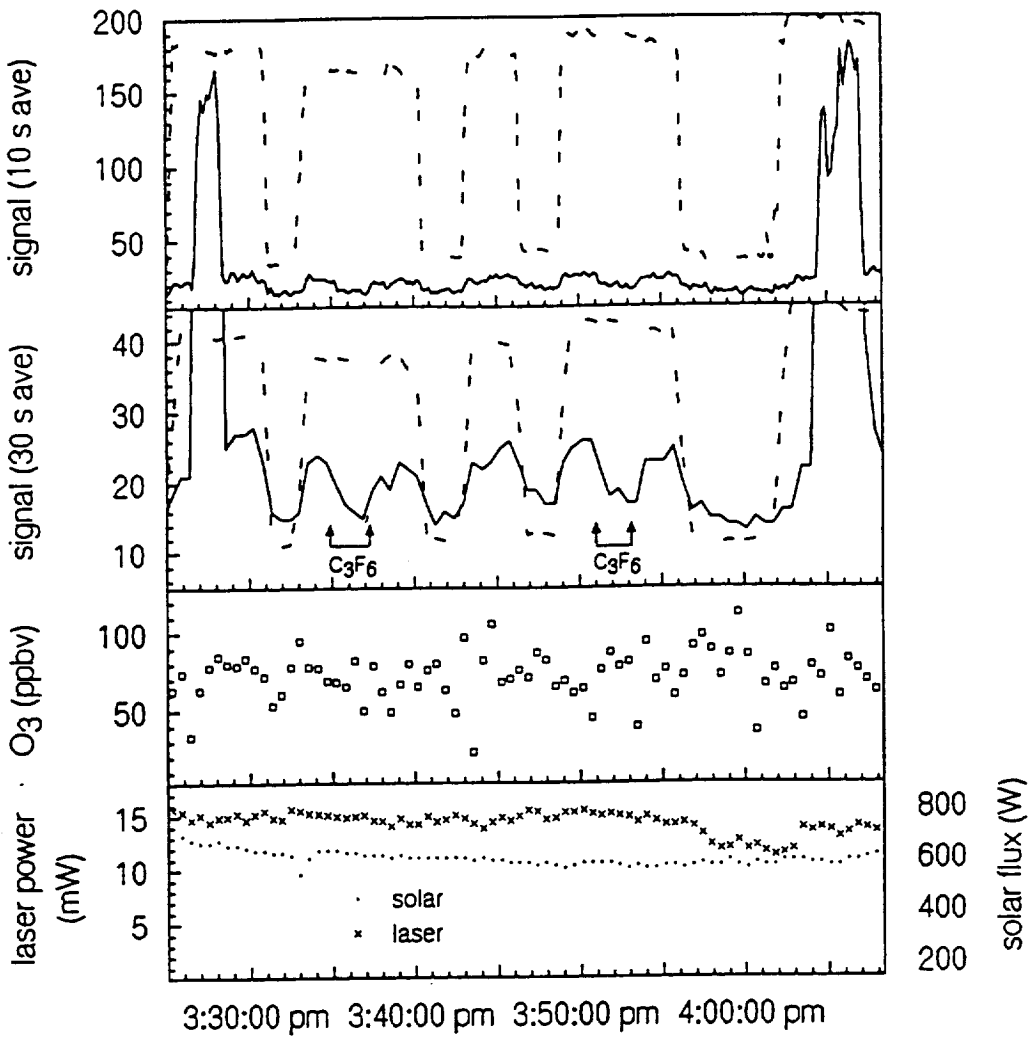

Figure 9. OH and HO_2 data from September 17, 1991, taken on the roof of the Walker Building on the Penn State campus. Shown are the OH and HO_2 signals (solid line), the reference cell signal (dashed line), O_3, laser power and solar flux. Perfluoropropylene was added at the times shown.

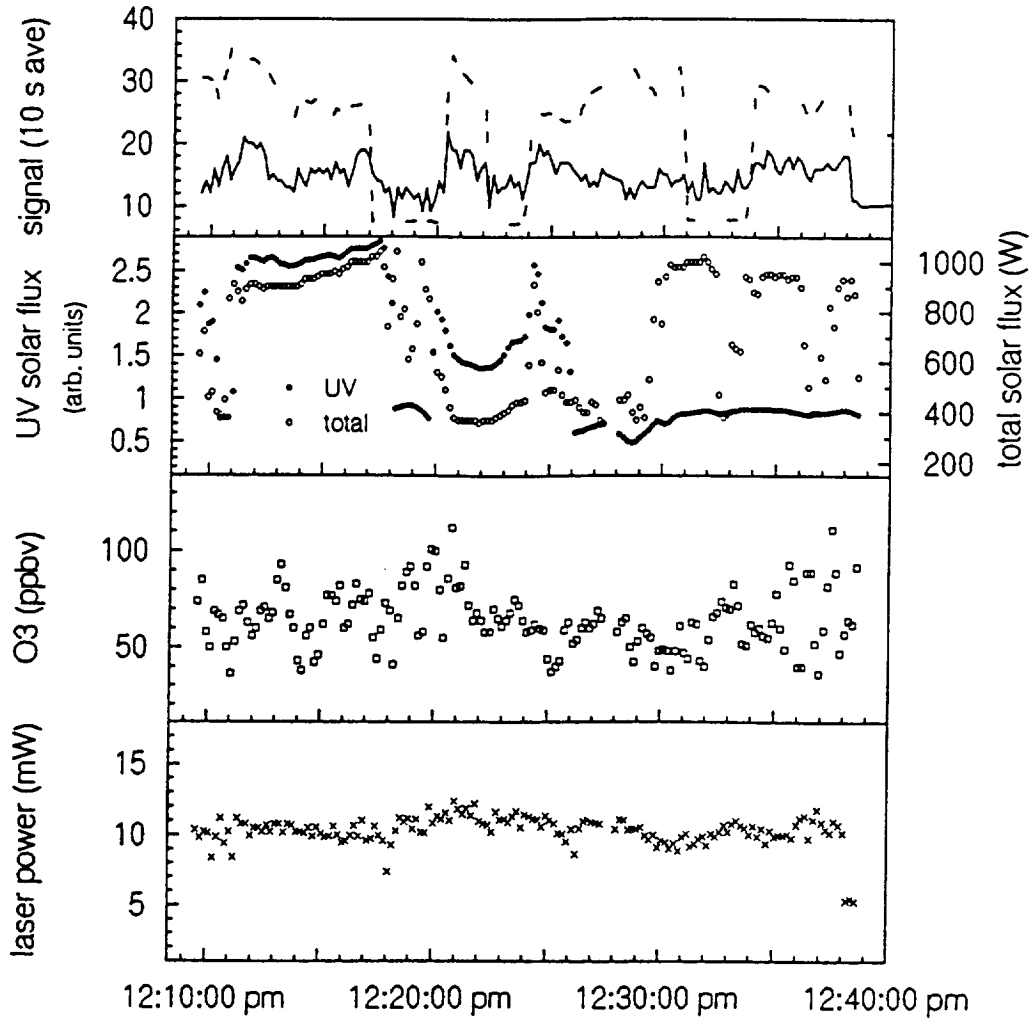

Figure 10. Sample of a 30-minute segment of data taken on September 17, 1991. Shown are the OH signal (solid line), the reference cell signal (dashed line), UV solar flux (filled circles, arbitrary units), total solar flux (open circles), O_3 and laser power. Note the correlation between the OH signal and the UV solar flux.

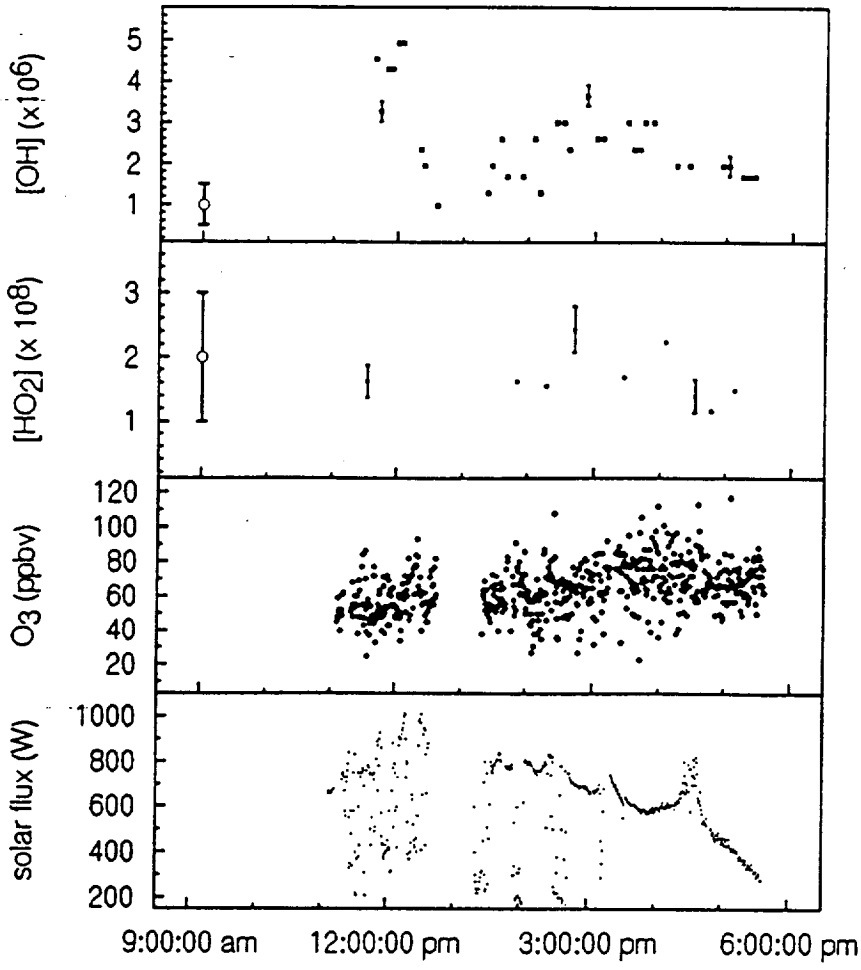

Figure 11. Measurements of OH and HO_2 (5-min averages) as a function of time of day on September 17, 1991 from the roof of the Walker Building. Samples of the statistical errors associated with each measurement of OH and HO_2 are shown on various points. Absolute error is indicated on the left of each plot.

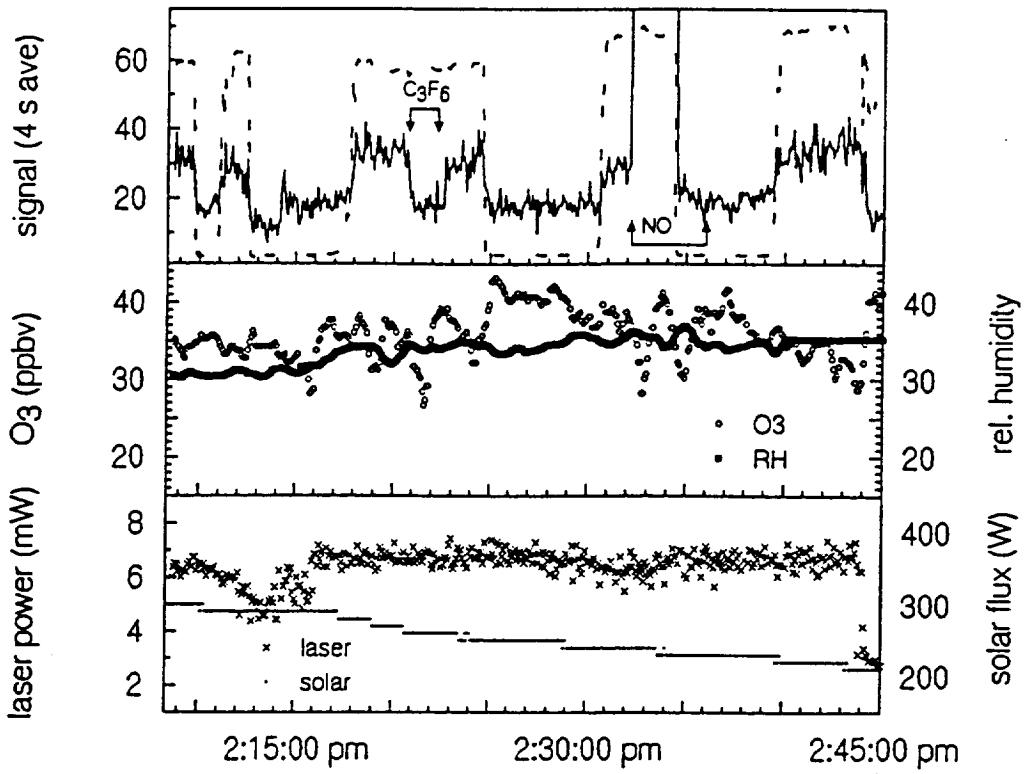

Figure 12. OH and HO_2 data from March 18, 1992 from the roof of the Walker Building. Shown are the OH signal (solid line), the reference cell signal (dashed line), O_3, relative humidity, laser power, and solar flux. C_3F_6 and NO were added at the times shown.

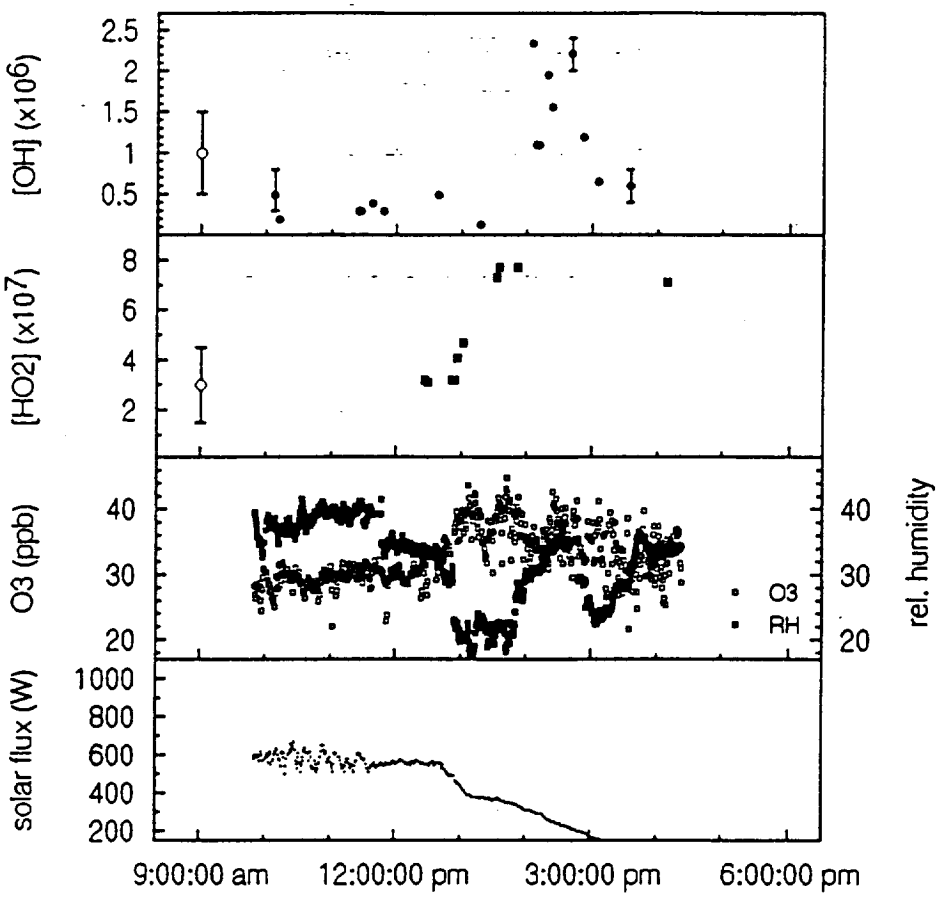

Figure 13. Measurements of OH and HO_2 (5-min averages) as a function of time of day on March 18, 1992 from the roof of the Walker Building. Samples of the statistical errors associated with each measurement of OH are shown on various points. Statistical error for the HO_2 measurements are smaller than the points themselves. Absolute error is indicated on the left of each plot.